nature materials

REVIEW ARTICLE

PUBLISHED ONLINE: 22 JULY 2011 | DOI: 10.1038/NMAT3064

# Thermal properties of graphene and nanostructured carbon materials

Alexander A. Balandin

**Recent years have seen a rapid growth of interest by the scientific and engineering communities in the thermal properties of materials. Heat removal has become a crucial issue for continuing progress in the electronic industry, and thermal conduction in low-dimensional structures has revealed truly intriguing features. Carbon allotropes and their derivatives occupy a unique place in terms of their ability to conduct heat. The room-temperature thermal conductivity of carbon materials span an extraordinary large range — of over five orders of magnitude — from the lowest in amorphous carbons to the highest in graphene and carbon nanotubes. Here, I review the thermal properties of carbon materials focusing on recent results for graphene, carbon nanotubes and nanostructured carbon materials with different degrees of disorder. Special attention is given to the unusual size dependence of heat conduction in two-dimensional crystals and, specifically, in graphene. I also describe the prospects of applications of graphene and carbon materials for thermal management of electronics.**

The recent increasing importance of the thermal properties of materials is explained both by practical needs and fundamental science. Heat removal has become a crucial issue for continuing progress in the electronic industry owing to increased levels of dissipated power. The search for materials that conduct heat well has become essential for design of the next generation of integrated circuits and three-dimensional (3D) electronics[1]. Similar thermal issues have been encountered in optoelectronic and photonic devices. Alternatively, thermoelectric energy conversion requires materials that have a strongly suppressed thermal conductivity[2].

A material's ability to conduct heat is rooted in its atomic structure, and knowledge of thermal properties can shed light on other materials' characteristics. The thermal properties of materials change when they are structured on a nanometre scale. Nanowires do not conduct heat as well as bulk crystals owing to increased phonon-boundary scattering[3] or changes in the phonon dispersion[4]. At the same time, theoretical studies of heat conduction in two-dimensional (2D) and one-dimensional (1D) crystals have revealed exotic behaviour that leads to infinitely large intrinsic thermal conductivity[5,6]. The thermal-conductivity divergence in 2D crystals means that unlike in bulk, the crystal anharmonicity alone is not sufficient for restoring thermal equilibrium, and one needs to either limit the system size or introduce disorder to have the physically meaningful finite value of thermal conductivity. These findings have led to discussions of the validity of Fourier's law in low-dimensional systems[7,8].

Carbon materials, which form a variety of allotropes[9], occupy a unique place in terms of their thermal properties (Fig. 1a). Thermal conductivity of different allotropes of carbon span an extraordinary large range — of over five orders of magnitude — from ~0.01 W mK$^{-1}$ in amorphous carbon to above 2,000 W mK$^{-1}$ at room temperature in diamond or graphene. In type-II diamond, thermal conductivity reaches 10,000 W mK$^{-1}$ at a temperature of approximately 77 K. The thermal conductivity of carbon nanotubes (CNTs) — ~3,000–3,500 W mK$^{-1}$ at room temperature[10,11] — exceeds that of diamond, which is the best bulk heat conductor.

The exfoliation of graphene[12] and discovery of its exotic electrical conduction[13–15] made possible, among other things, the first experimental study of heat transport in strictly 2D crystals. The availability of high-quality few-layer graphene (FLG) led to experimental observations of the evolution of thermal properties as the system dimensionality changes from 2D to 3D. The first measurements of the thermal properties of graphene[16–19], which revealed a thermal conductivity above the bulk graphite limit, ignited strong interest in the thermal properties of this material and, in a more general context, heat conduction in crystals of lower dimensionality. A rapidly increasing number of publications on the subject, often with contradictory results, calls for a comprehensive review. Such a review with an emphasis on graphene is particularly appropriate, because this material provided the recent stimulus for thermal research, and it may hold the key to understanding heat conduction in low dimensions. These considerations motivated this review, which discusses the thermal properties of graphene and CNTs in the context of carbon allotropes.

## Basics of heat conduction

Before discussing the detailed properties of nanocarbon materials, it is essential to define the main quantities of heat conduction and outline the nanoscale size effects. Thermal conductivity is introduced through Fourier's law, $q = -K\nabla T$, where $q$ is the heat flux, $K$ is the thermal conductivity and $\nabla T$ is the temperature gradient. In this expression, $K$ is treated as a constant, which is valid for small temperature ($T$) variations. In a wide temperature range, $K$ is a function of $T$. In anisotropic materials, $K$ varies with crystal orientation and is represented by a tensor[20–22].

In solid materials heat is carried by acoustic phonons — that is, ion-core vibrations in a crystal lattice — and electrons so that $K = K_p + K_e$, where $K_p$ and $K_e$ are the phonon and electron contributions, respectively. In metals, $K_e$ is dominant owing to large concentrations of free carriers. In pure copper — one of the best metallic heat conductors — $K \approx 400$ W mK$^{-1}$ at room temperature and $K_p$ is limited to 1–2% of the total. Measurements of the electrical conductivity ($\sigma$) define $K_e$ via the Wiedemann–Franz law, $K_e/(\sigma T) = \pi^2 k_B^2/(3e^2)$, where $k_B$ is the Boltzmann constant and $e$ is the charge of an electron. Heat conduction in carbon materials is usually dominated by phonons, even for graphite[23], which has metal-like properties[24].

Department of Electrical Engineering and Materials Science and Engineering Program, Bourns College of Engineering, University of California, Riverside, California 92521, USA. e-mail: balandin@ee.ucr.edu

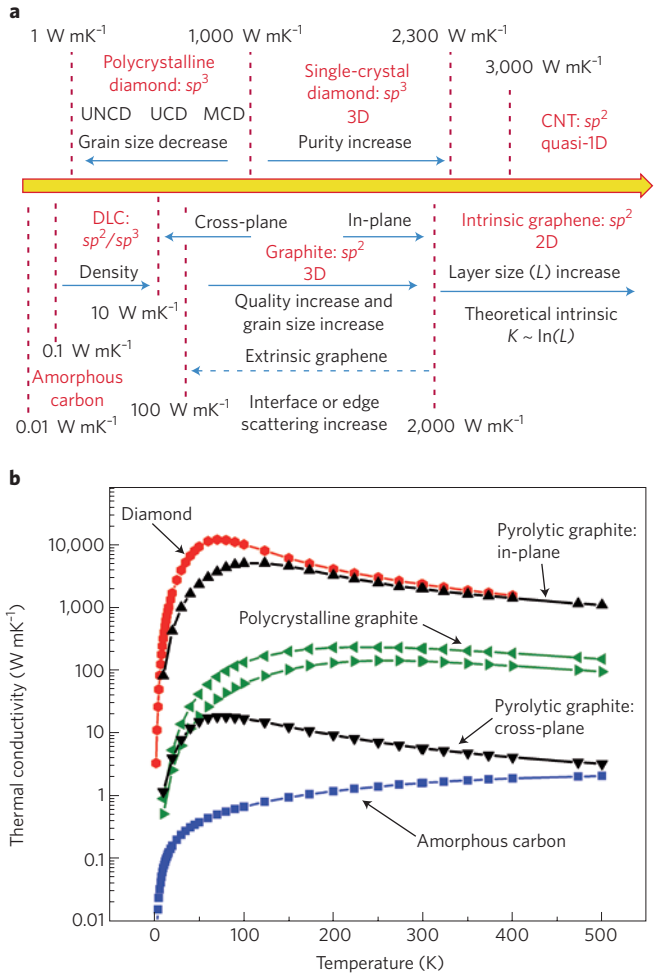


**Figure 1 | Thermal properties of carbon allotropes and their derivatives.** **a**, Diagram based on average values reported in literature. The axis is not to scale. **b**, Thermal conductivity of bulk carbon allotropes as a function of $T$. The plots are based on commonly accepted recommended values from ref. 29. The curve 'diamond' is for the electrically insulating type-II diamond; 'polycrystalline graphite' is for AGOT graphite — a high-purity pitch-bonded graphite; and 'pyrolytic graphite' is for high-quality graphite analogous to HOPG. Note an order of magnitude difference in $K$ of pyrolytic graphite and polycrystalline graphite with disoriented grains. The $K$ value for pyrolytic graphite constitutes the bulk graphite limit of ~2,000 W mK$^{-1}$ at room temperature. At low $T$, $K$ is proportional to $T\gamma$, where $\gamma$ varies over a wide range depending on graphite's quality and crystallite size[29,30].

This is explained by the strong covalent $sp^2$ bonding resulting in efficient heat transfer by lattice vibrations. However, $K_e$ can become significant in doped materials.

The phonon thermal conductivity is expressed as $K_p = \Sigma_j \int C_j(\omega) v_j^2(\omega) \tau_j(\omega) d\omega$. Here $j$ is the phonon polarization branch, that is, two transverse acoustic branches and one longitudinal acoustic branch; $\upsilon$ is the phonon group velocity, which, in many solids, can be approximated by the sound velocity; $\tau$ is the phonon relaxation time, $\omega$ is the phonon frequency and $C$ is the heat capacity. The phonon mean-free path ($\Lambda$) is related to the relaxation time as $\Lambda = \tau\upsilon$. In the relaxation-time approximation, various scattering mechanisms, which limit $\Lambda$, are additive — that is, $\tau^{-1} = \Sigma\tau_i^{-1}$, where $i$ enumerates the scattering processes. In typical solids, the acoustic phonons, which carry the bulk of heat, are scattered by other phonons, lattice defects, impurities, conduction electrons and interfaces[22,25,26]. A simpler equation for $K_p$, derived from the kinetic theory of gases, is $K_p = (1/3)C_p\upsilon\Lambda$, where $C_p$ is the specific heat capacity.

It is important to distinguish between diffusive and ballistic phonon-transport regimes. The thermal transport is called diffusive if the size of the sample, $L$, is much larger than $\Lambda$, that is, phonons undergo many scattering events. When $L < \Lambda$ the thermal transport is termed ballistic. Fourier's law assumes diffusive transport. Thermal conductivity is called intrinsic when it is limited by the crystal-lattice anharmonicity. The crystal lattice is anharmonic when its potential energy has terms higher than the second order with respect to the ion displacements from equilibrium. The intrinsic $K$ limit is reached when the crystal is perfect, without defects or impurities, and phonons can only be scattered by other phonons, which 'see' each other owing to anharmonicity. The anharmonic phonon interactions, which lead to finite $K$ in three dimensions, can be described by the Umklapp processes[22]. The degree of crystal anharmonicity is characterized by the Gruneisen parameter $\gamma$, which enters the expressions for the Umklapp scattering rates[22,25]. Thermal conductivity is extrinsic when it is mostly limited by the extrinsic effects, such phonon-rough-boundary or phonon-defect scattering.

In nanostructures, $K$ is reduced by scattering from boundaries, which can be evaluated as[27] $1/\tau_B = (\upsilon/D)((1-p)/(1+p))$. Here $\tau_B$ is the phonon lifetime and $1/\tau_B$ is the phonon scattering rate, $D$ is the nanostructure or grain size and $p$ is the specularity parameter defined as a probability of specular scattering at the boundary. The momentum-conserving specular scattering ($p = 1$) does not add to thermal resistance. Only diffuse phonon scattering from rough interfaces ($p \to 0$), which changes the momentum, limits $\Lambda$. One can find $p$ from the surface roughness or use it as a fitting parameter to experimental data. When the phonon-boundary scattering is dominant, $K$ scales with $D$ as $K_p \sim C_p\upsilon\Lambda \sim C_p\upsilon^2\tau_B \sim C_p\upsilon D$. In nanostructures with $D << \Lambda$, phonon dispersion can undergo modifications owing to confinement resulting in changes in $\upsilon$ and more complicated size dependence[28]. $C_p$ is defined by the phonon density of states, which leads to different $C_p(T)$ dependence in 3D, 2D and 1D systems, and reflected in the $K(T)$ dependence at low $T$ (refs 22,27). For example, in bulk at low $T$, $K(T)$ is ~$T^3$, whereas it is ~$T^2$ in 2D systems.

## Bulk carbon allotropes

Revisiting the thermal properties of bulk carbon allotropes — graphite, diamond and amorphous carbon — provides proper reference for the discussion of graphene and nanostructured carbons. It also helps to distinguish new physics emerging in low-dimensional structures from mundane material-quality issues. It is hard to find another material where $K$ has been studied as rigorously as it has in graphite. One of the reasons for this was the needs of the nuclear industry. Ironically, the data for graphite are sometimes difficult to find because the studies were conducted in the last century and often published in reports of limited circulation. Correspondingly, there is confusion among modern-day researchers about what is the $K$ value for basal planes of high-quality graphite. Figure 1b shows $K$ values for two types of high-purity graphite ($sp^2$ bonding), diamond ($sp^3$) and amorphous carbon (disordered mixture of $sp^2$ and $sp^3$). These plots are based on the recommended values reported in ref. 29, which were obtained by compilation and analysis of hundreds of research papers with conventionally accepted experimental data.

Pyrolytic graphite, which is similar to highly oriented pyrolytic graphite (HOPG), has an in-plane $K$ of ~2,000 W mK$^{-1}$ at room temperature. Its cross-plane $K$ is more than two orders of magnitude smaller. Another type of chemically pure pitch-bonded graphite, produced by different technique, has an order-of-magnitude-smaller in-plane $K$ of ~200 W mK$^{-1}$. The $K$ anisotropy is much less pronounced. This difference is explained by the fact that HOPG is made from large crystallites, which are well aligned with each other, so that the overall behaviour is similar to that of a single crystal[30]. Pitch-bonded graphite is also polycrystalline, but the crystal axes are not highly oriented and the grain boundaries are more pronounced[30]. As a result, $K$ values of polycrystalline graphite of

the types other than HOPG can be strongly limited by the grain size $D$. The same factors limit $K$ in graphene prepared by chemical vapour deposition (CVD), which is polycrystalline with misoriented grains[31,32]. Thus, I consider a $K$ value of ~2,000 W mK$^{-1}$ as the graphite room-temperature bulk limit. Any smaller value is indicative of a lower-quality graphite, where $K$ is limited by phonon scattering on grain boundaries, defects or rough sample edges. The experimental $K$ values for HOPG are in excellent agreement with theoretical predictions for the intrinsic $K$ of graphite[23,33].

In all bulk carbon allotropes, heat is mostly carried by acoustic phonons. In diamond and HOPG, $K$ attains its maximum at ~70 K and ~100 K, respectively. For higher $T$, $K$ decreases as ~1/$T$, which is characteristic of crystalline solids, where $K$ is limited by phonon Umklapp scattering. In amorphous carbon $K$ varies from ~0.01 W mK$^{-1}$ at $T$ = 4K to ~2 W mK$^{-1}$ at $T$ = 500 K. It increases monotonically with $T$, which is expected for disordered materials, where the heat-conduction mechanism is the hopping of localized excitations[34]. As seen from Fig. 1b, $K$ for HOPG and pitch-bonded graphite has a different $T$ dependence at low temperature. It is well known that $K(T)$ dependence in graphite varies substantially. It is defined not only by the phonon density of states through $C_p$, but also by graphite's grain size and quality[29,30].

## Disordered and nanostructured carbons

Let us discuss the thermal properties of materials where $K$ is limited by disorder or grain boundaries rather than by the intrinsic lattice dynamics. An important representative of this class of materials is diamond-like carbon (DLC), which is a metastable form of amorphous carbon containing a significant fraction of $sp^3$ bonds[35]. DLC films are widely used as protective coatings with optical windows for magnetic storage disks and in biomedical applications. DLC consists of amorphous carbon and hydrogenated alloys. Hydrogen-free DLC with the highest $sp^3$ content is called tetrahedral amorphous carbon. Experimental studies[36–42] revealed that heat conduction in DLC is mostly governed by the amount and structural disorder of the $sp^3$ phase. If the $sp^3$ phase is amorphous, $K$ scales approximately linearly with the $sp^3$ content, density and elastic constants (Fig. 2a). Polymeric and graphitic DLC films have the lowest $K$, ~0.1–0.3 W mK$^{-1}$; hydrogenated tetrahedral amorphous carbon has a $K$ value of ~1 W mK$^{-1}$; and tetrahedral amorphous carbon has the highest $K$, which can go up to ~10 W mK$^{-1}$ at room temperature[41]. Among amorphous solids, tetrahedral amorphous carbon is probably the material with the highest $K$ (refs 35,36). If the $sp^3$ phase orders — even in small grains such as in nanocrystalline diamond — a strong $K$ increase occurs for a given density, Young's modulus and $sp^3$ content.

Progress in polycrystalline diamond films prepared by CVD — ultrananocrystalline (UNCD), nanocrystalline (NCD) and microcrystalline (MCD) (Fig. 2b) — renewed interest in their thermal properties[43,44]. Most studies of polycrystalline diamond[45–51] agree that $K$ depends strongly on $D$ and covers the range from ~1–10 W mK$^{-1}$ in UNCD to ~550 W mK$^{-1}$ in MCD ($D \approx 3$–4 μm). The grain-size dependence can be estimated from $K_p \approx (1/3)C\upsilon D$, which assumes

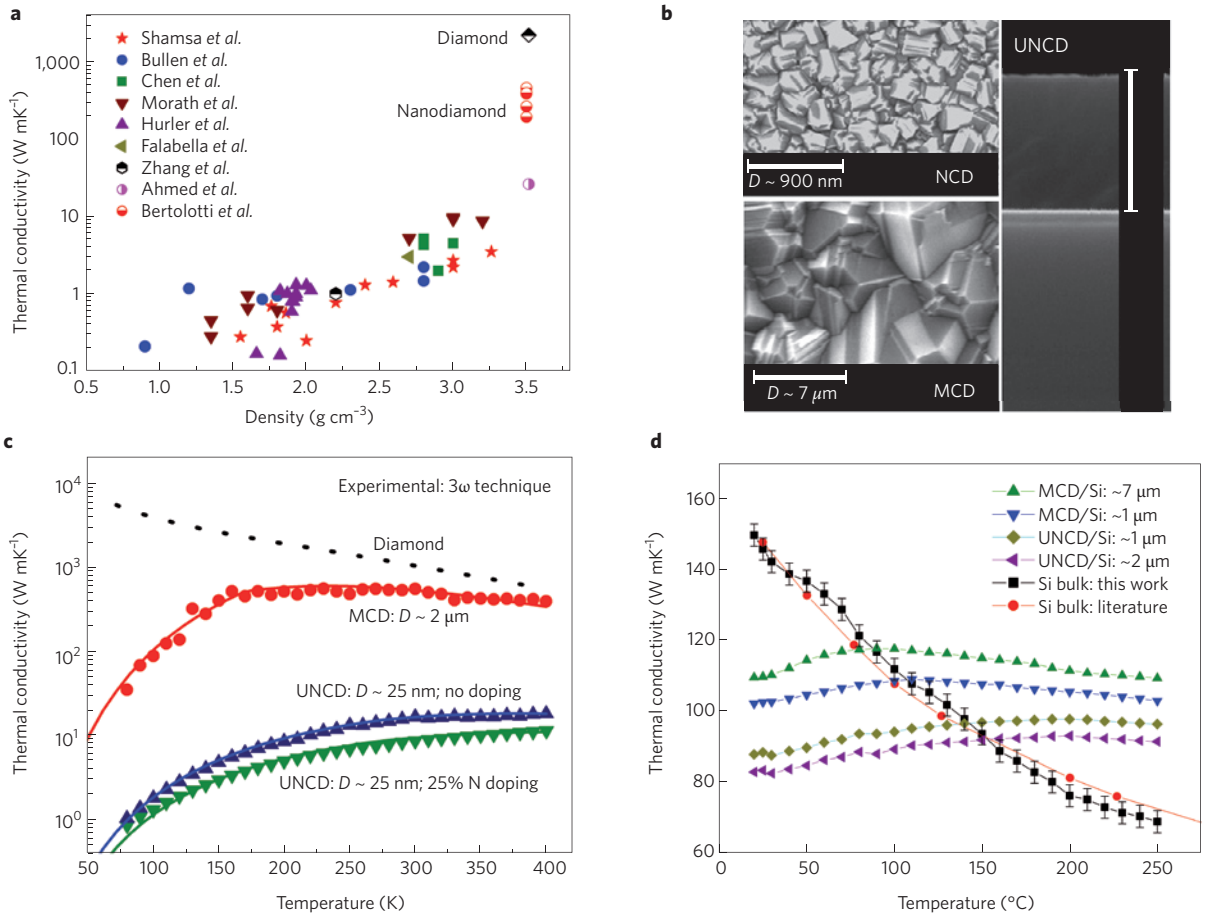


**Figure 2 | Thermal conductivity of disordered and nanostructured carbon materials. a**, $K$ of DLC as a function of mass density. Note that ordering of the $sp^3$ phase inside grains in NCD results in a significant $K$ increase. **b**, Scanning electron microscopy images showing the UNCD/Si interface and grain sizes in NCD and MCD. Scale bars 2 μm. **c**, Comparison of $K$ temperature dependence for UNCD and MCD films. **d**, Effective thermal conductivity of MCD/Si and UNCD/Si composite substrates indicating that they can outperform Si wafers at elevated $T$ in terms of thermal properties. Panels adapted with permission from: **a**, ref. 41, © 2006 AIP; **c**, ref. 51, © 2008 AIP; **d**, ref. 55, © 2010 AIP.

that inside the grain, phonon propagation is the same as in the bulk crystal. This was confirmed by the high-resolution measurements of local $K$ in polycrystalline diamond[46,47]. A more accurate theoretical description can be achieved with the relaxation-time approximation through the introduction of the scattering on grain boundaries and defects inside the grains[52]. The phonon-hopping model[53], which involves phonon transmission through grain boundaries, gave good agreement for polycrystalline diamond with different $D$ (Fig. 2c). Some studies suggested that heat conduction can be different in UNCD with ultrasmall $D$ (~3–5 nm), where thermal transport is controlled by the intrinsic properties of the grain boundaries[49]. The grain boundaries contain the $sp^2$-phase as opposed to the $sp^3$-phase carbon inside the grains[54].

Applications of polycrystalline diamond films for heat spreading in integrated circuits can become feasible if thermal resistance of the composite Si/polycrystalline diamond substrate becomes smaller than that of Si wafers. There are trade-offs in optimizing Si/polycrystalline diamond substrates. MCD films have higher $K$ because of the larger grains, but suffer from a rough interface with Si, which increases the thermal resistance of the structure. UNCD forms better interfaces, but has few-nanometre size grains. Recent developments mark progress in this direction (Fig. 2d). It has been shown that composite Si/polycrystalline diamond substrates, which are more thermally resistive at room temperature, outperform Si wafers at elevated temperatures (above ~360 K), which are characteristic for the operation of electronic devices[55].

## Carbon nanotubes

Thermal transport in CNTs and graphene, unlike in NCD or DLC, can be dominated by the intrinsic properties of the strong $sp^2$ lattice, rather than by phonon scattering on boundaries or by disorder, giving rise to extremely high $K$ values[10,11,16,17]. From the theoretical point of view, CNTs are similar to graphene, but have large curvatures and different quantization conditions for phonon modes. In the discussion of heat conduction in CNTs, one has to take into account the ambiguity of the intrinsic $K$ definition for 2D and 1D systems[5–8,56–62]. Although graphene is structurally simpler, I start with experimental data for CNTs because their thermal properties have been studied for more than a decade. CNTs became the first nanostructures with reported experimental $K$ exceeding that of bulk graphite and diamond.

Table 1 summarizes experimental data for single-walled CNTs (SWCNTs) and multi-walled CNTs (MWCNTs)[10,11,63–66]. Theoretical results[67–70] are also provided for comparison. There is substantial data scatter in the reported room temperature $K$ values for CNTs ranging from ~1,100 $mK^{-1}$ (ref. 71) to ~7,000 W $mK^{-1}$ (ref. 64). The highest $K$ values obtained in the experiments were attributed to the ballistic transport regime achieved in some CNTs. Commonly quoted values for individual CNTs are ~3,000 W $mK^{-1}$ for MWCNTs (ref. 10) and ~3,500 W $mK^{-1}$ for SWCNTs (ref. 11) at room temperature. These values are above the bulk-graphite limit of ~2,000 W $mK^{-1}$. Thus, CNTs are nanostructures where heat transport is not mostly limited by the extrinsic effects, such as boundary scattering, like in many semiconductor nanowires with rough interfaces.

The largest $\Lambda$ extracted from the measurements[10,64] was ~700–750 nm at room temperature. As the length of the measured CNTs was above 2 μm, the phonon transport was still diffusive, but close to the ballistic transition. At $T < 30$ K the energy-independent $\Lambda$ of ~0.5–1.5 mm was extracted from measurements for SWCNT bundles[63]. The peak in $K$ of CNTs was achieved at $T \approx 320$ K (ref. 10), which is a substantially higher temperature compared with bulk crystals. This indicates that Umklapp phonon

**Table 1 | Thermal conductivity of graphene and carbon nanotubes.**

| Sample | $K$ (W $mK^{-1}$) | Method | Comments | Refs |
|---|---|---|---|---|
| MWCNT | >3,000 | Electrical; micro-heater | Individual; diffusive; suspended | 10 |
| SWCNT | ~3,500 | Electrical self-heating | Individual; boundary | 11 |
| SWCNT | 1,750–5,800 | Thermocouples | Bundles; diffusive | 63 |
| SWCNT | 3,000–7,000 | Electrical; micro-heater | Individual; ballistic; suspended | 64 |
| CNT | 1,100 | Electrical; micro-heater | Individual; suspended | 71 |
| CNT | 1,500–2,900 | Electrical | Individual | 65 |
| CNT | ~6,600 | Theory: molecular dynamics | $K_{CNT} < K_G$ | 66 |
| CNT | ~3,000 | Theory: molecular dynamics | Strong defect dependence | 67 |
| SWCNT | ~2,500 | Theory: Boltzmann transport equation | $K_{CNT} < K_G$ | 69 |
| SWCNT | ~7,000 | Theory: molecular dynamics and Boltzmann transport equation | $L > 20$ nm | 70 |
| Graphene | ~2,000–5,000 | Raman optothermal | Suspended; exfoliated | 16, 17 |
| FLG | ~1,300–2,800 | Raman optothermal | Suspended; exfoliated; $n = 4$–2 | 74 |
| Graphene | ~2,500 | Raman optothermal | Suspended; CVD | 75 |
| Graphene | 1,500–5,000 | Raman optothermal | Suspended; CVD | 77 |
| Graphene | 600 | Raman optothermal | Suspended; exfoliated; $T \approx 660$ K | 76 |
| FLG ribbon | 1,100 | Electrical self-heating | Supported; exfoliated; $n < 5$ | 79 |
| Graphene | 600 | Electrical | Supported; exfoliated | 78 |
| Graphene | 2,000–5,000 | Theory: valence force field, Boltzmann transport equation, $\gamma(q)$ | Strong width dependence | 83 |
| Graphene | 1,000–5,000 | Theory: relaxation-time approximation, $\gamma_{TA}$, $\gamma_{LA}$ | Strong size dependence | 62 |
| Graphene | 8,000–10,000 | Theory: molecular dynamics, Tersoff | Square graphene sheet | 84 |
| Graphene | 1,400–2,400 | Theory: Boltzmann transport equation | Length dependence | 69 |
| Graphene | ~4,000 | Theory: ballistic | Strong width dependence | 86 |

$\gamma(q)$, Gruneisen parameter dependent on the phonon wave vector; $\gamma_{LA}$ and $\gamma_{TA}$, Gruneisen parameter averaged separately for LA and TA phonon modes. The data is for near room temperature unless otherwise specified.

**Box 1 | Measurement of the thermal conductivity of graphene.**

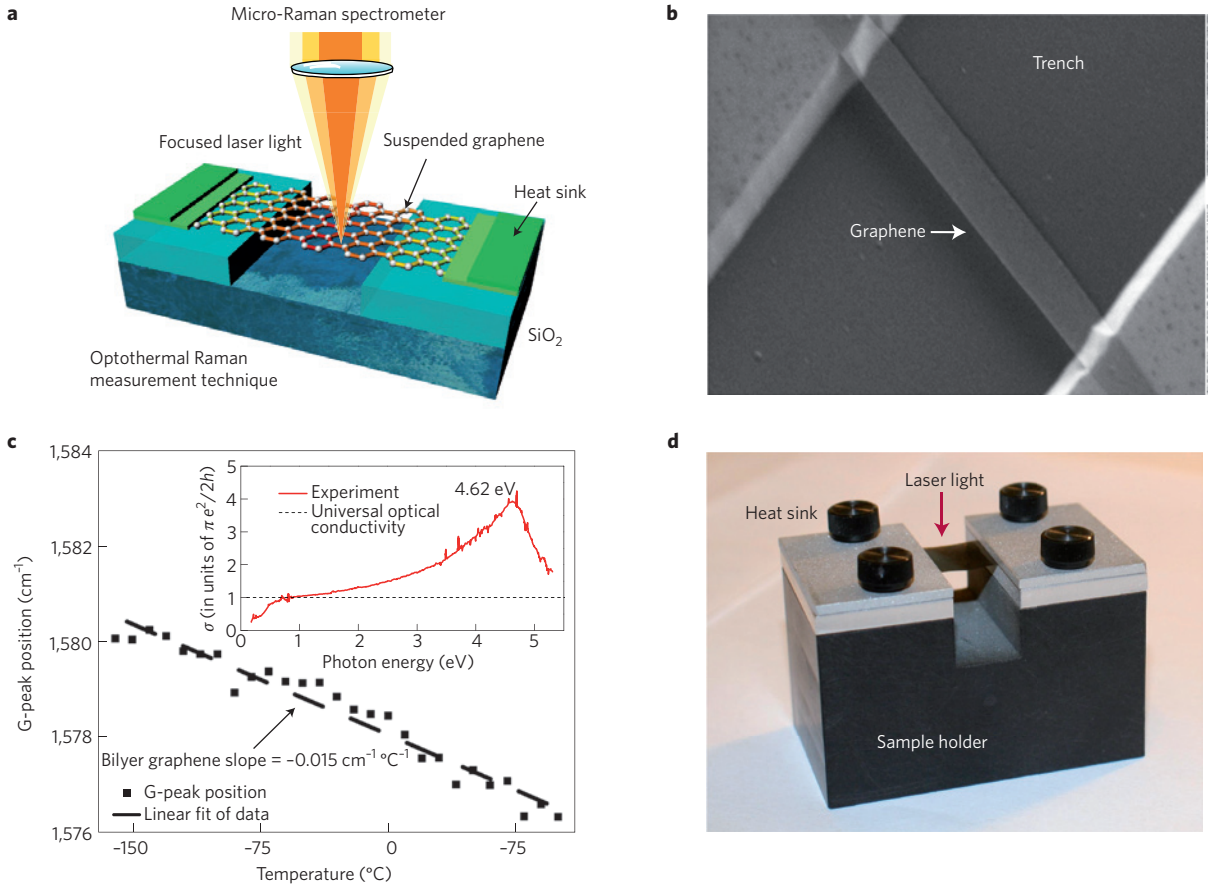


Methods of measuring thermal conductivity ($K$) can be divided into two groups: steady state and transient[20]. In transient methods, the thermal gradient is recorded as a function of time, enabling fast measurements of the thermal diffusivity ($D_T$) over large $T$ ranges. $C_p$ and mass density ($\rho_m$) have to be determined independently to calculate $K = D_T C_p \rho_m$. If $K$ determines how well a material conducts heat, $D_T$ tells us how quickly a material conducts heat. Although many methods rely on electrical means for supplying heating power and measuring $T$, there are other techniques where the power is provided by light. In many steady-state methods, $T$ is measured by thermocouples. The transient 3ω technique for thin films[21] uses $T$ dependence of electrical resistivity for $K$ extraction.

The first experimental study of heat conduction in graphene was made possible by developing an optothermal Raman technique (panel **a**). The heating power $\Delta P$ was provided by a laser light focused on a suspended graphene layer connected to heat sinks at its ends (for example, panel **b** shows FLG with $n = 2$ of rectangular shape suspended across a 3-μm-wide trench in a Si wafer). Temperature rise ($\Delta T$) in response to $\Delta P$ was determined with a micro-Raman spectrometer. The G peak in graphene's Raman spectrum exhibits strong $T$ dependence. Panel **c** presents the temperature shift in bilayer graphene. The inset shows that the optical absorption in graphene is a function of the light wavelength owing to many-body effects[94]. The calibration of the spectral position of the G peak with $T$ was performed by changing the sample temperature while using very low laser power to avoid local heating[18]. The frequency of the G peak ($\omega_G$) as a function of temperature — calibration curve $\omega_G(T)$ — allows one to convert a Raman spectrometer into an 'optical thermometer'. During $K$ measurements, the suspended graphene layer is heated by increasing laser power. Local $\Delta T$ in graphene is determined by $\Delta T = \Delta\omega_G/\xi_G$, where $\xi_G$ is the $T$ coefficient of the G peak. The amount of heat dissipated in graphene can be determined either by measuring the integrated Raman intensity of the G peak, as in the original experiments[16], or by a detector placed under the graphene layer, as in the follow-up experiments[75]. As optical absorption in graphene depends on the light wavelength[94] (panel **c**, inset) and can be affected by strain, defects, contaminations and near-field or multiple reflection effects for graphene flakes suspended over the trenches, it is essential to measure absorption under the conditions of the experiment.

A correlation between $\Delta T$ and $\Delta P$ for graphene samples with a given geometry gives a $K$ value through solution of the heat-diffusion equation. Large graphene layers ensure the diffusive-transport regime. The suspended portion of graphene is essential for determining $\Delta P$, forming a 2D heat front propagating towards the heat sinks, and reducing thermal coupling to the substrate. The method allows one to monitor the temperature of the Si and $SiO_2$ layers near the trench with suspended graphene from the shift in the position of Si and $SiO_2$ Raman peaks[17]. This can be used to determine the thermal coupling of graphene to the $SiO_2$ insulating layer. The optothermal Raman technique for measuring the $K$ of graphene is a direct steady-state method. It can be extended to other suspended films (panel **d**), for example, graphene films[19], made of materials with pronounced temperature-dependent Raman signatures. Panel **c** adapted with permission from ref. 20, © 2007 ACS; inset reproduced with permission from ref. 94, © 2011 APS.

scattering is suppressed in CNTs over a wide temperature range. At low $T$, $K(T)$ follows the temperature dependence of $C_p$. For individual MWCNTs, $K(T)$ of $\sim T^{2.5}$ was observed[10], which is similar to bulk graphite[29]. In SWCNT bundles the $K(T)$ dependence was linear for $T < 30$ K (ref. 63). The thermoelectric measurements with SWCNTs revealed a Seebeck coefficient of ~42 μV K$^{-1}$ at room temperature, which is about an order of magnitude higher than that of graphite or metals, suggesting that electron transport is not ballistic[64].

The measured thermal conductance $G_p$ in SWCNTs was found to increase with temperature from $0.7 \times 10^{-9}$ W K$^{-1}$ or $\sim 7g_0$ at 110 K to $3.8 \times 10^{-9}$ W K$^{-1}$ or $\sim 14g_0$ at room temperature[64], where $g_0 = \pi^2 k_B^2 T/3h \approx (9.456 \times 10^{-9}\,\mathrm{W\,K^{-2}})T$ is the universal quantum of thermal conductance and represents the maximum possible conductance per phonon mode[72]; $h$ is Planck's constant. Assuming different diameters of CNTs ($d_{CNT}$) in the range from 1 nm to 3 nm, the extracted $K$ of SWCNTs was found to change from ~8,000 to ~2,500 W mK$^{-1}$ at room temperature[64]. An experimental study reported decreasing $K$ in MWCNTs from ~2,800 to ~500 W mK$^{-1}$, with the outer diameter increasing from 10 nm to ~28 nm (ref. 65). The same $K$ dependence on $d_{CNT}$ was reported in ref. 71. This experimental trend for MWCNTs suggests that the interactions of phonons and electrons between multi-walled layers affect $K$. Thermal conductivity increases as the number of atomic walls in MWCNTs decreases[65]. Interestingly, the Boltzmann transport equation predicts increasing $K$ with increasing diameter for SWCNTs when $1 < d_{CNT} < 8$ nm (ref. 69).

## Experimental studies of graphene

The first experimental studies[16,17,73,74] of the thermal conductivity of graphene were carried out at the University of California, Riverside (see Box 1). The optothermal Raman measurements were performed with large-area suspended graphene layers exfoliated from high-quality HOPG. The authors found $K$ exceeding ~3,000 W mK$^{-1}$ near room temperature, that is, above the bulk graphite limit, observed $K$ dependence on the layer size and determined that $K_e << K_p$. The phonon mean-free path was estimated to be ~775 nm near room temperature[17]. A following independent study[75] also used the Raman technique, but modified it by addition of a power meter under the suspended portion of graphene. It was found that the $K$ of suspended high-quality graphene prepared by CVD exceeded ~2,500 W mK$^{-1}$ at 350 K, and it was as high as ~1,400 W mK$^{-1}$ at 500 K (experimental uncertainty ~40%)[75]. The reported value is larger than the $K$ of bulk graphite at room temperature. Another group that repeated the optothermal Raman measurements found $K \approx 630$ W mK$^{-1}$ for suspended graphene at $T \approx 600$ K (ref. 76). The graphene membrane was heated to $T = 660$ K in the centre and above ~500 K over most of its area. Since $K$ decreases with $T$, this fact can explain the difference between refs 16, 17 and 75, which reported $K$ near room temperature. Differences in strain distribution in the suspended graphene of various sizes and geometries may also affect the results. Other optothermal studies with suspended graphene found $K$ in the range from ~1,500 to ~5,000 W mK$^{-1}$ (ref. 77).

The data for suspended or partially suspended graphene is closer to the intrinsic $K$ because suspension reduces thermal coupling to the substrate and scattering on the substrate defects and impurities. It also helps to form the in-plane heatwave front, which allows one to obtain the data pertinent to graphene itself rather than to the graphene/substrate interface even if only a part of the layer is suspended. For practical applications, it is important to know the $K$ of supported graphene, that is, graphene attached to the substrate along its entire length. The measurements for exfoliated graphene on $SiO_2$/Si revealed an in-plane $K$ of ~600 W mK$^{-1}$ near room temperature[78]. This value is below those reported for suspended graphene, but it is still rather high, exceeding the $K$ of Si (145 W mK$^{-1}$) and Cu (400 W mK$^{-1}$). Solving the Boltzmann transport equation, the authors determined the $K$ of free graphene to be ~3,000 W mK$^{-1}$ near room temperature. They attributed the reduced experimental value to graphene–substrate coupling and phonon leaking across the interface[78]. An independent study, which used an electrical self-heating method, found $K \approx$ 1,000–1,400 W mK$^{-1}$ near room temperature for graphene nanoribbons with less than five atomic planes and a width between 16 nm and 52 nm (ref. 79). The breakdown current density of graphene was measured to be ~$10^8$ A cm$^{-2}$, close to that of CNTs. This study assumed that the thermal resistance of the graphene/substrate interface is the same as that of SWCNT/substrate interface rather than measuring it[79]. Table 1 provides representative experimental data for suspended and supported graphene.

## Few-layer graphene

It is interesting to examine the evolution of the thermal properties of FLG with increasing thickness, $H$ (number of atomic planes, $n$). One has to clearly distinguish two cases: thermal transport limited by (1) intrinsic properties of the FLG lattice, that is, crystal anharmonicity; and (2) extrinsic effects, for example, by phonon-boundary or defect scattering. The optothermal Raman study[74] found that $K$ of suspended uncapped FLG decreases with increasing $n$, approaching the bulk graphite limit (Fig. 3a). This evolution of $K$ was explained by considering the intrinsic quasi-2D crystal properties described by the phonon Umklapp scattering[74]. As $n$ in FLG increases, the phonon dispersion changes and more phase-space states become available for phonon scattering leading to a decrease in $K$. The phonon scattering from the top and bottom boundaries in suspended FLG is limited if constant $n$ is maintained over the layer length. The small thickness of FLG ($n < 4$) also means that phonons do not have a transverse component in their group velocity ($v_\perp = 0$) leading to even weaker $1/\tau_B$ term for phonon scattering from the top and bottom boundaries. In FLG films with $n > 4$ the boundary scattering can increase, because $v_\perp \neq 0$, and it is harder to maintain constant $n$ through the whole area of a FLG flake, resulting in $K$ below the graphite limit. The graphite value recovers for thicker films. One should note that experimental data points in Fig. 3a are normalized to the same width (5 μm). It is not possible to obtain a set of high-quality damage-free FLG samples with varying $n$ and identical width and shape. The normalization procedure was described in detail in ref. 74.

Experimentally observed evolution of heat conduction in FLG with $n$ varying from 1 to ~4 (ref. 74) is in qualitative agreement with the theory for crystal lattices described by the Fermi–Pasta–Ulam Hamiltonians[56]. Recent non-equilibrium molecular-dynamics calculations for graphene nanoribbons with $n$ from 1 to 8 (ref. 80) gave the thickness dependence $K(n)$ in excellent agreement with the experiment[74]. As seen in Fig. 3b, $K$ saturates near bulk graphite's value at $n \sim 4$–7. The authors did not observe $K$ dependence on the nanoribbon width because $W << \Lambda$ and perfectly periodic boundary conditions were assumed for the edges (that is, $p = 1$). Strong quenching of $K$ as $n$ changes from 1 to 2 is in line with the earlier theoretical predictions[66]. It is also consistent with the experimental dependence of $K$ on the outer diameter in MWCNTs[65,71]. Another group solved the Boltzmann transport equation under the assumption that in-plane interactions are described by the Tersoff potential, whereas the Lennard–Jones potential models interactions between atoms belonging to different layers[81]. They obtained a strong $K$ decrease as $n$ changed from 1 to 2 and a slower decrease for $n > 2$.

The situation is entirely different for encased graphene where thermal transport is limited by the acoustic phonon scattering from the top and bottom boundaries and disorder, which is unavoidable when FLG is embedded between two layers of dielectrics. A study[82], conducted with the 3ω technique, found $K \approx 160$ W mK$^{-1}$ for encased single-layer graphene at $T = 310$ K. It increases to ~1,000 W mK$^{-1}$ for graphite films with $H \approx 8$ nm (Fig. 3c). It was also found that for a given $H$, the suppression of $K$ in encased graphene, as compared with bulk graphite, was stronger at low temperature ($T < 150$ K) where $K \sim T^\beta$ ($\beta$ is a constant in the range $1.5 < \beta < 2$)[82]. Thermal conduction

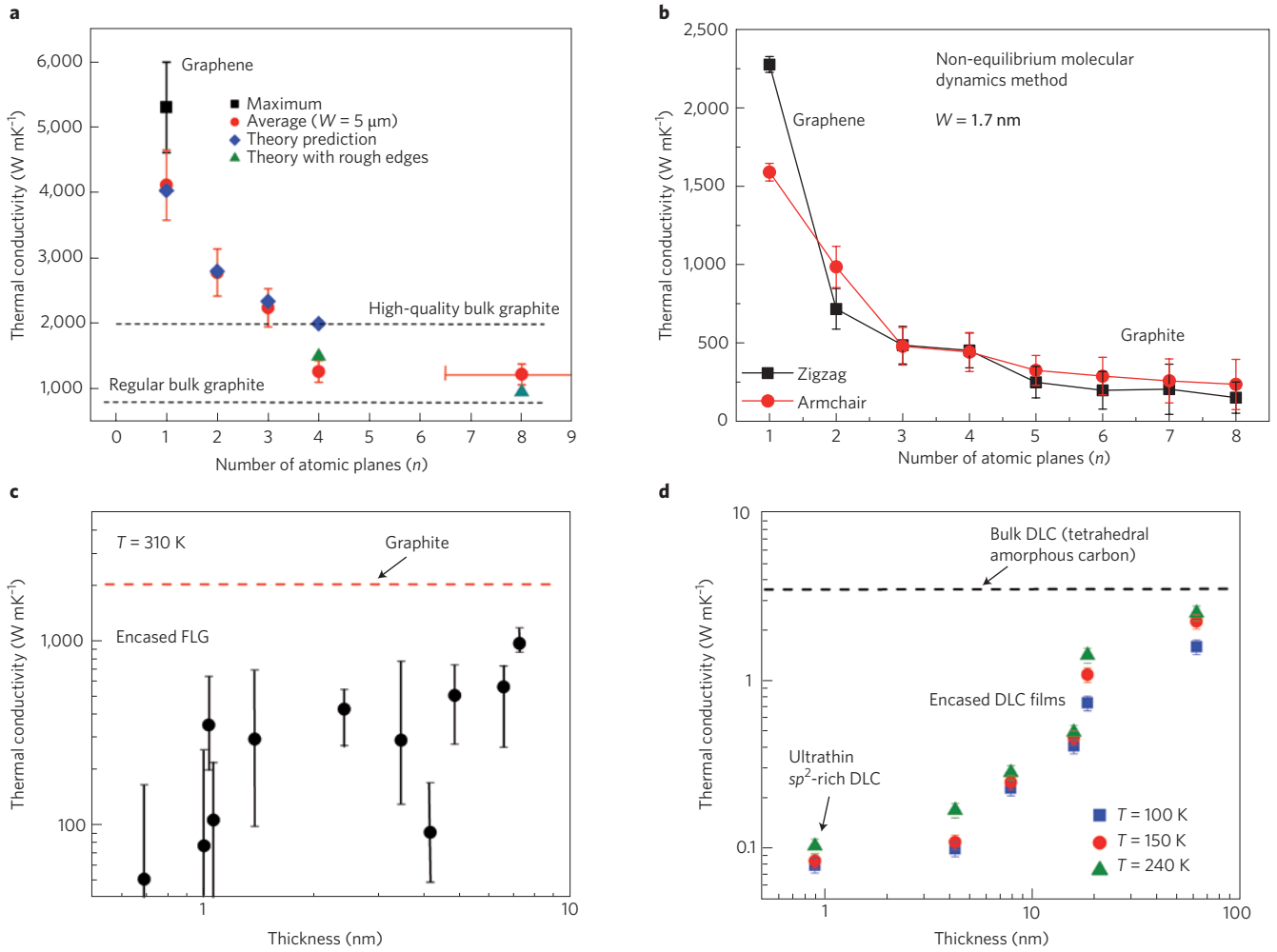


**Figure 3 | Thermal conductivity of quasi-2D carbon materials: intrinsic versus extrinsic effects. a**, Measured and calculated thermal conductivity of suspended FLG as a function of $n$ (at the fixed flake width, $W$). For $n > 4$, $K$ can drop below the bulk graphite limit owing to the onset of the phonon-boundary scattering from the top and bottom interfaces; $K$ recovers for sufficiently thick films. **b**, Thermal conductivity of graphene nanoribbons obtained from molecular dynamics simulations as a function of $n$ showing a similar trend. **c**, Measured $K$ of encased FLG as a function of $H$. The transport is dominated by the phonon-boundary scattering and disorder resulting in characteristic $K$ scaling with $H$. **d**, Thermal conductivity of encased ultrathin DLC films as a function of $H$, indicating a similar trend to the encased FLG. Panels adapted with permission from: **a**, ref. 74 © 2010 NPG; **b**, ref. 80, © 2011 AIP; **c**, ref. 82, © 2010 ACS. Panel **d**, based on data from ref. 42.

in encased FLG was limited by rough-boundary scattering and disorder penetration throughout the graphene. The presence of the evaporated oxide on top of the graphene is known to cause defects in the graphene layer. Correspondingly, $K$ dependence on $H$ was similar to other material systems where $K$ is extrinsically limited and scales with $H$. In conventional crystalline thin films, where $H < \Lambda$, but still much larger than the lattice constant, $K$ grows with $H$ as $K \approx CvH$ until it reaches the bulk limit $K \approx Cv\Lambda$. A similar scaling with $H$ was observed for encased FLG (Fig. 3c) and ultrathin DLC films (Fig. 3d). The overall values of $K$ in encased DLC films are much smaller than those for encased FLG, as expected for more disordered materials, but the $K(H)$ trend is essentially the same. In ultrathin DLC, the interface layers are known to be the mostly disordered $sp^2$ phase[42]. In both encased FLG and ultrathin DLC films, the scaling cannot follow exactly the same dependence as in crystalline films because of the influence of disorder and changes of the material properties with $H$.

## Theory of graphene and CNTs

Measurements of the thermal properties of graphene stimulated a surge of interest in theoretical studies of heat conduction in graphene and graphene nanoribbons[83–91]. The high-quality suspended FLG also made possible experimental testing of theoretical results obtained for heat conduction in 2D lattices[56–60]. Theoretical description of the thermal properties of 2D graphene is closely related to that of CNTs[69]. When analysing theoretical results one needs to take into account differences between the ballistic ($L < \Lambda$) and diffusive ($L > \Lambda$) transport regimes, and specifics of the intrinsic thermal conductivity in 2D systems (Box 2) related to $K$ divergence with the system size.

Thermal conductivity of graphene was addressed, for the first time, within the framework of the relaxation-time approximation[23,61]. It was shown that the intrinsic $K$ of graphene should exceed that of bulk graphite when the lateral size of the graphene layer becomes sufficiently large (Box 2). The Klemens theory predicted that the Umklapp-limited $K$ in graphene has logarithmic divergence with the layer or grain size. Substrate coupling reduced $K$ by increased phonon leakage to the substrate and phonon scattering[23,61]. The analytical expression for graphene was obtained as a special case of the bulk graphite theory[33], with the principal difference being the fact that in graphene the contribution of the low-energy phonons is not limited by cut-off phonon frequency and extends all the way to zero frequency[23,61]. The theory gave excellent agreement with experimental data for graphite under the assumption that heat is carried mostly by

longitudinal acoustic (LA) and transverse acoustic (TA) phonons, and contributions of out-of-plane acoustic (ZA) phonons are negligible due to their small group velocity ($v \to 0$) in the Brillouin zone centre and large $\gamma$ (refs 23,33,61). The modified theory with $\gamma$, determined independently for LA and TA modes, provided excellent agreement with experimental data for graphene (Box 2). Addition of realistic

**Box 2 | Unique features of heat conduction in two-dimensional crystals.**

Investigation of heat conduction in graphene[16,17] and CNTs[8] raised the issue of ambiguity in the definition of intrinsic thermal conductivity for 2D and 1D crystal lattices. It is now accepted that $K$ limited by the crystal anharmonicity alone, referred to as intrinsic, has a finite value in 3D bulk crystals[6,56]. However, the intrinsic $K$ reveals a logarithmic divergence in 2D crystals, $K \sim \ln(N)$, and power-law divergence in 1D systems, $K \sim N^{\alpha}$, with the system size $N$ (where $N$ is number of atoms; $0 < \alpha < 1$)[6,7,56–60]. This anomalous behaviour, which leads to infinite $K$ in 1D and 2D systems, is principally different from the ballistic heat conduction in structures smaller in size than the phonon mean-free path. The logarithmic divergence can be removed by the introduction of extrinsic scattering mechanisms, such as scattering on defects, or by pinning (for example, coupling to substrates)[56]. Alternatively, one can define the intrinsic $K$ of 2D crystals for a given size. There have been indications that for very large lattices the finite value of intrinsic $K$ can be regained in CNTs or graphene owing to the higher-order phonon scattering processes. Nevertheless, this has not been conclusively proven yet, and the ambiguity in $K$ is a principally new situation from what we are accustomed to in the 3D world.

The uniqueness of heat conduction in graphene can be illustrated with an expression, derived by Klemens, for the intrinsic Umklapp-limited thermal conductivity of graphene[23,61]:

$$K = (2\pi\gamma^2)^{-1}\rho_m(v^4/f_m T)\ln(f_m/f_B)$$

Here $f_m$ is the upper limit of the phonon frequencies defined by the phonon dispersion, and $f_B = (Mv^3 f_m/4\pi\gamma^2 k_B TL)^{1/2}$, where $M$ is the mass of an atom, is the size-dependent low-bound cut-off frequency for acoustic phonons, introduced by limiting the phonon mean-free path with the graphene layer size $L$. Klemens[23,61] neglected the contributions of out-of-plane acoustic phonons because of their low group velocity and large $\gamma$. The phonon dispersion and $\gamma$ in graphene are shown in panels **a** and **b**, respectively. On these figures, one can see longitudinal optical (LO), transverse optical (TO), out-of-plane optical (ZO), longitudinal acoustic (LA), transverse acoustic (TA) and out-of plane acoustic (ZA) phonon polarization branches. The fundamental $K$ dependence on $L$ obtained from this model is illustrated in panel **c**; $\gamma_{LA}$ and $\gamma_{TA}$ are Gruneisen parameters averaged separately for each phonon branch. This result is in line with other theoretical approaches[6,7,56–60], which numerically confirmed that $K$ diverges in 2D anharmonic lattices[56]. Panel **d** shows that anharmonicity is sufficient to have a finite intrinsic $K$ value in 3D crystals (the running slope $\alpha_N$ extracted from $K(N)$ dependence goes to zero in the 3D case, but saturates in 1D and 2D cases). The intrinsic $K$ is defined for an ideal graphene without defects. In experiments, $K$ is also limited by extrinsic factors, for example, point defects, grain boundaries, substrate coupling and so on, and does not grow to unphysically high values. Panels adapted with permission from: **a**, ref. 83, © 2009 APS; **b**, ref. 136, © 2005 APS; **c**, ref. 62, © 2009 AIP; **d**, ref. 56, © 2010 APS.

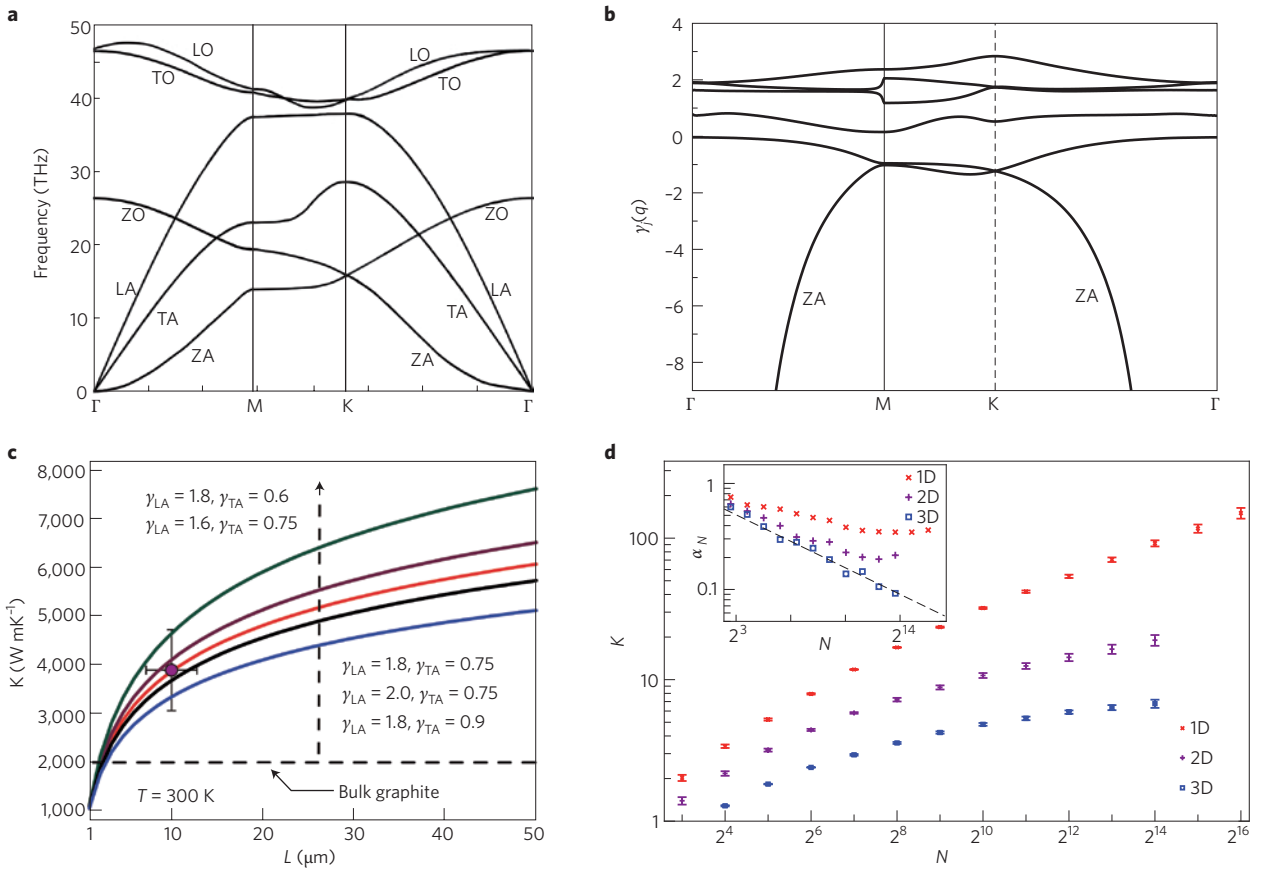

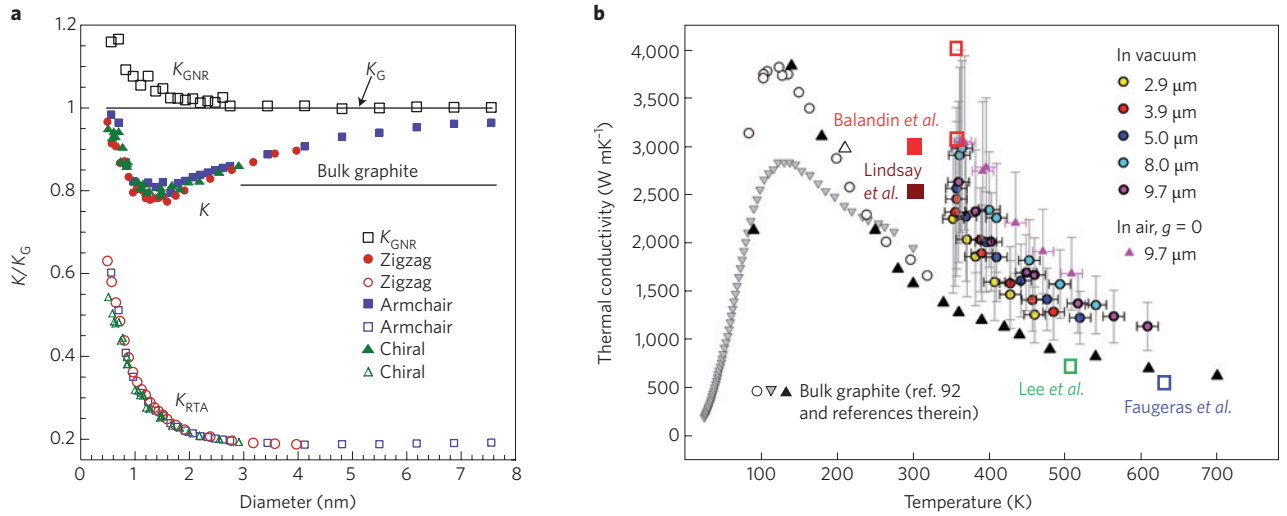


**Figure 4 | Thermal properties of low-dimensional carbon materials. a**, Calculated thermal conductivity of CNTs and graphene indicating that the intrinsic $K$ of CNTs is always lower than that of graphene. $K_{RTA}$ is the thermal conductivity calculated within the relaxation-time approximation; $K_{GNR}$ is the thermal conductivity of graphene nanoribbon. Adapted with permission from ref. 69, © 2010 APS. **b**, Experimental thermal conductivity of graphene as a function of temperature. Adapted with permission from ref. 92, © 2011 ACS. Experimental data points from other works are indicated by empty rectangular boxes: red from refs. 16,17,74; green from ref. 93; blue from ref. 76. The filled red and brown boxes are theoretical data points from refs. 62 and 69, respectively. These two points are for different graphene flake sizes — 3 μm and 5 μm, respectively. Setting $L$ = 3 μm in ref. 62 would give $K \approx 2{,}500$ W mK$^{-1}$ as in ref. 69. Note that the experimental results from different research groups obtained for graphene by the Raman optothermal technique are in agreement within the experimental uncertainty of the method.

concentrations of defects in the framework of the relaxation-time approximation, allows one to remove the logarithmic divergence of $K$ and obtain meaningful results for graphene[83].

The first equilibrium and non-equilibrium molecular-dynamics simulations determined $K \approx 6{,}600$ W mK$^{-1}$ for (10,10) CNTs and even higher $K \approx 9{,}000$ W mK$^{-1}$ for graphene near room temperature[66]. It was noted that once graphene layers are stacked in graphite, the interlayer interactions quench the $K$ of the system by an order of magnitude[66]. In the past few years, a number of molecular-dynamics studies, with Tersoff and Brenner potentials, addressed heat conduction in graphene nanoribbons with various length, edge roughness and defect concentration[84–91]. A recent molecular-dynamics study found $K \approx 8{,}000$–$10{,}000$ W mK$^{-1}$ at room temperature for square graphene sheets, which was size independent for $L > 5$ nm (ref. 84). For the ribbons with fixed $L$ = 10 nm and width varying from 1 to 10 nm, $K$ increased from ~1,000 W mK$^{-1}$ to 7,000 W mK$^{-1}$. Thermal conductivity in graphene nanoribbons with rough edges can be suppressed by orders of magnitude compared with that in graphene nanoribbons with perfect edges[84,87]. Table 1 summarizes the $K$ calculated for graphene using different approaches.

An interesting question, which has practical implications, is which carbon low-dimensional material — CNTs or graphene — has a higher intrinsic $K$. A recent theoretical study[69] has found that $K$ of SWCNTs ($K_{CNT}$) is always below that of graphene ($K_G$) for $d_{CNT} > 1$ nm (Fig. 4a). The calculation included contributions from all phonon modes — TA, LA and ZA. $K_{CNT}$ was found to be ~$0.8 \times K_G$ for CNTs with $d_{CNT} \approx 1.5$ nm, and gradually increased with $d_{CNT}$ approaching $K_G$ for $d_{CNT} \approx 8$ nm (ref. 69). The calculated $K(d_{CNT})$ is a non-monotonic function, which gives ~2,500 W mK$^{-1}$ at room temperature for $L$ = 3 μm. The ballistic limit for $K_G$ was found to be as high as 12,800 W mK$^{-1}$.

## Theoretical and experimental uncertainties

An intriguing open question in the theory of phonon transport in graphene is the relative contribution to heat conduction by LA, TA and ZA phonon polarization branches (Box 2). There have been opposite views expressed as to the importance of ZA phonons, from negligible[23,33,61] to dominant[69,78,81,85]. The argument against ZA contributions originates from Klemens' theory, which states that ZA modes have large $\gamma$ (refs 22,23,61) — which defines the scattering strength — and zero group velocity near the zone centre, resulting in a negligible contribution to heat transport[23,33,61]. The argument for the strong contributions of ZA modes is made on the basis of a selection rule in ideal graphene, which restricts the phase space for phonon-phonon scattering, and increases the lifetime of ZA modes[85]. However, graphene placement on any substrates and the presence of nanoscale corrugations in the graphene lattice can break the symmetry selection rule, which restricts ZA phonon scattering. It is also possible that ZA dispersion undergoes modification, for example, linearization, owing to the substrate coupling. An answer to the question of relative contributions may take time, considering that after almost a century of investigations there are still debates about the contributions of LA and TA phonons in conventional semiconductors. The measurements of $T^{\beta}$ dependence alone cannot provide evidence in favour of one or the other phonon contribution, because $K(T)$ dependence in graphite is known to depend strongly on the material quality[29,30,82].

To directly compare independent measurements of $K_G$, I have reproduced measured $K(T)$ from ref. 92, and added experimental[16,17,76,93] and theoretical[62,83] data from other works (Fig. 4b). In this plot, $K$ is larger for graphene than graphite. At $T > 500$ K the difference becomes less pronounced, which is expected as the higher phonon energy levels become populated. Note that some studies have not measured the absorption under the experimental conditions[76,93]. The accuracy of determining the power absorbed in graphene may substantially affect $K$ values in the optical techniques. It was recently found that optical absorption in graphene is a strong function of wavelength owing to the many-body effects[94], which can lead to different absorption in optothermal experiments (Box 1, panel c, inset). The absorption of 2.3% is observed in the near-infrared at ~1 eV. Absorption steadily increases for energies higher than 1.5 eV. The 514.5-nm and 488-nm Raman laser lines correspond to 2.41 eV and 2.54 eV, respectively. The assumption of 2.3% in the Raman measurements with $\lambda > 1.5$ eV leads to underestimated $K$.

So far, the highest values of $K_G$ were measured with the Raman optothermal technique. It is difficult to directly compare its accuracy

**Table 2 | Thermal conductivity enhancement in nanocarbon composites.**

| Filler | Enhancement | Volume fraction | Base material | Refs |
|---|---|---|---|---|
| MWCNT | 160% | 1.0 vol.% | Oil | 105 |
| SWCNT | 125% | 1.0 wt% | Epoxy | 106 |
| SWCNT | 200% | 5.0 wt% | Epoxy | 108 |
| Graphite nanoplatelets | 3,000% | 25.0 vol.% | Epoxy | 109 |
| Graphene oxide nanoparticles | 30–80% | 5.0 vol.% | Glycol; paraffin | 110 |
| Graphene oxide | 400% | 5.0 wt% | Epoxy resin | 111 |
| Graphene | 500% | 5.0 vol.% | Silver epoxy | 112 |
| Graphene | 1,000% | 5.0 vol.% | Epoxy | 112 |

with that of the thermal-bridge or 3ω techniques[21,39–42] when they are applied to graphene. The Raman technique used for graphene[16,17,74–77] has the benefits of relative ease of sample preparation and reduced sample contamination. However, its temperature resolution is substantially inferior to the 20–50 mK sensitivity, which can be achieved with the resistance temperature detectors. The Raman data for graphene is often reported with up to 40% uncertainty in the absolute $K$ value. At the same time, the assembly of suspended graphene between two suspended micro-thermometers makes such measurements extremely challenging, and results in ambiguity related to the influence of the residual polymeric layers and other defects created during fabrication. More work has to be done with the suspended micro-thermometers to have an accurate assessment of the systematic errors in the various techniques (see Outlook).

One should keep in mind that comparison of $K$ of graphene and graphite contains ambiguity related to the definition of the graphene thickness $h_C$. Most studies used $h_C = 0.34$ nm defined by the carbon-bond length. However, this definition is not unique[95,96]. One can introduce $h_C$ from the inter-atomic potential[95] or start from Young's modulus and tensile strength[96] obtaining $h_C$ in the range from 0.06 to 0.69 nm, which can shift the $K$ of graphene up and down, compared with the bulk graphite value[83]. This means that consistent use of $h_C = 0.34$ nm allows for comparison of the results obtained for graphene in different groups. However, it leaves ambiguity when comparing the $K$ for graphene and graphite. Although the theoretical evidence and results of the optothermal Raman measurements suggest that the $K$ of graphene can exceed that of graphite, a particular choice of $h_C$ can shift the $K$ curves up or down in Figs 3 and 4.

## Graphene/substrate interfaces

Thermal boundary resistance ($R_B$) at the interface of graphene with other materials is a subject of both fundamental science and practical interest. Knowledge of $R_B$ can help in understanding graphene thermal coupling to matrix materials. Controlling $R_B$ is important for graphene's electronic- and thermal-management applications. It is defined as $R_B = (q/\Delta T)^{-1}$, where $\Delta T$ is the temperature difference between two sides of the interface. It has a non-zero value even at the perfect interfaces owing to differences in the phonon density of states — an effect known as Kapitza thermal resistance[97]. The actual $R_B$ is usually higher than the Kapitza resistance owing to interface imperfections.

Heat conduction across graphene or FLG has been measured by several different techniques, including electrical 3ω (ref. 98), Raman-electrical[99,100], and optical pump-and-probe[101] methods. The thermo-reflectance technique was used to study the graphite interface with Cr, Al, Ti and Au (ref. 102). The room temperature $R_B$ of ~$10^{-8}$ Km$^2$ W$^{-1}$ was found in most cases. The studies are in agreement that neither the cross-plane conductance nor $R_B$ reveal a strong dependence on the thickness of FLG or the nature of the dielectric or metal substrate. $R_B$ decreases with $T$ following a typical trend for Kapitza resistance[97].

A first-principle calculation of heat transfer between graphene and $SiO_2$, which treated the graphene–substrate coupling as a weak van-der-Waals-type interaction, determined the heat transfer coefficient of ~$2.5 \times 10^7$ W m$^{-2}$ K$^{-1}$ (ref. 103). This translates to $R_B$ of ~$4 \times 10^{-8}$ Km$^2$ W$^{-1}$, which is close to experimental data. Despite agreement on the average $R_B$, most studies note a significant sample-to-sample variation at the graphene/$SiO_2$ interface (for example, factor of ~4 for FLG with $n = 5$ in ref. 100). This means that graphene thermal coupling to other materials can depend strongly on the surface roughness, presence or absence of suspended regions in graphene layers, and methods of graphene preparation. Molecular-dynamics simulations found that $R_B$ at the graphene/oil interface is similar or smaller than that at graphene/solid interfaces[104–107]. The low $R_B$ of graphene with many materials is good news for graphene applications in thermal interface materials (TIMs).

## Thermal interface materials

The need for improved TIMs in modern electronics and optoelectronics stimulated interest in carbon materials as fillers for TIMs[105–113]. Current TIMs are based on polymers or greases filled with thermally conductive particles such as silver, which require high volume fractions of filler (up to 70%) to achieve $K$ of ~1–5 W mK$^{-1}$ for the composite. Carbon materials that were studied as fillers include CNTs, graphite nanoplatelets, graphene oxide nanoparticles and graphene flakes derived by chemical processes. The thermal conductivity enhancement factor $\eta = (K_{eff} - K_{base})/K_{base}$, where $K_{eff}$ is thermal conductivity of the composite material and $K_{base}$ is thermal conductivity of the initial base material, for composites is shown in Table 2.

Despite variations in $\eta$, explained by different base materials and preparation methods, the conclusion is that graphene, CNTs and graphene oxide nanoparticles are promising as fillers in terms of the resulting $K_{eff}$. The enhancements are above 100% for 1 wt% of the CNT or graphene loading. This is not achievable with conventional fillers. Graphene demonstrated the highest $\eta$ owing to its geometry and better coupling to base materials[107,112]. Future TIM applications of carbon materials would depend on many factors, including the composite viscosity, coefficient of thermal expansion, $R_B$ and cost. For epoxy–graphene composites, the coefficient of thermal expansion was found to vary in the range ~(5–30) $\times 10^{-5}$ (per 1 °C) and decreased with increasing graphene fraction[111]. Carbon nanoparticles strongly enhance thermal diffusivity ($D_T$) of epoxy to ~60 mm$^2$ s$^{-1}$ at 70 vol.% (ref. 114). An important characteristic for TIM applications of graphene is its high temperature stability, which was verified up to 2,600 K (ref. 115). The use of liquid-phase exfoliated graphene[116] in advanced TIMs could become the first industry application, which would require large quantities of this material[117].

## Thermoelectric effects in graphene

Experimental studies[118] demonstrated that graphene — with an electron mobility ranging from 1,000 to 7,000 cm$^2$ Vs$^{-1}$ — has a peak value for thermoelectric power (TEP) at ~80 μV K$^{-1}$ at room temperature. The TEP sign, which defines the majority of charge carriers, changed from positive to negative as the gate bias crossed the charge neutrality point. Similar results with a TEP of

~50–100 μV K$^{-1}$ were obtained in other experiments[119,120]. Theory gave consistent results[121]. It was established theoretically that TEP behaves as $1/(n_0)^{1/2}$ at high carrier density ($n_0$), but saturates at low densities. TEP scales with the normalized temperature $T/T_F$ and does not depend on the impurity densities ($T_F$ is Fermi temperature)[121]. Calculations[122] reproduced experimental results[100] for the Seebeck coefficient ($S$) ranging from ~10 to ~100 μV K$^{-1}$ for $T$ ranging from ~100 to ~300 K. The theoretical studies of the phonon-drag effects on TEP in bilayer graphene revealed a higher $S$ at low $T$ (ref. 123).

The efficiency of thermoelectric energy conversion is determined by the figure of merit, $ZT = S^2\sigma T/(K_e + K_p)$. Moderate values of $S$ mean that ZT can only be made practically relevant if $K$ is suppressed. Although graphene reveals extremely high intrinsic $K$, its dominant $K_p$ component can be efficiently suppressed by using graphene ribbons with rough edges or introducing disorder[87,124,125]. Theoretical studies suggest that ZT can be made as high as ~4 at room temperature in zigzag graphene nanoribbons[126]. For comparison, ZT in state-of-art thermoelectrics is ~1 at room temperature. The improvement in graphene nanoribbons' ZT results from strong suppression of $K_p$ owing to phonon-edge disorder scattering without substantial deterioration of electron transport[126]. Graphene with intentionally introduced lattice disorder, for example, through electron-beam irradiation[127] or charged impurities[128], could become an option for thermoelectric energy conversion. Graphene reveals interesting thermoelectric effects — it has a high $S$ compared with elemental semiconductors and the $S$ sign can be changed by the gate bias instead of doping. However, the possibility of graphene's thermoelectric applications is still a subject of debate.

## Outlook

Carbon materials reveal a unique range of thermal properties with $K$ varying from 0.01 W mK$^{-1}$ to above 3,000 W mK$^{-1}$ near room temperature. If needed, for example, for thermoelectric applications, $K$ of graphene can be tuned to a wide range by the introduction of disorder or edge roughness. The excellent heat-conduction properties of graphene are beneficial for all proposed electronic and photonic applications. The transparent FLG electrodes can perform the additional function of removing heat and improving the efficiency of photovoltaic solar cells through the reduction of its temperature under illumination. Similarly, FLG serving as interconnects in 3D electronics can simultaneously act as lateral heat spreaders[129]. The demonstrated $K$ enhancement of composites by addition of small volume fractions of liquid-phase exfoliated graphene is promising for TIM applications. Progress in graphene prepared by CVD growth on various substrates[130–132] gives hope that one would have a much better control of the thermal properties of supported or encased FLG. FLG lateral-heat spreaders deposited on GaN wafers and connected to heat sinks were shown to substantially reduce the temperature rise in the high-power density AlGaN/GaN field-effect transistors[133]. Moreover, even if one has to use thin graphite layers instead of single-layer graphene to prevent $K$ degradation, one would still benefit from the high in-plane $K \approx 2{,}000$ W mK$^{-1}$ of graphite, which is exceptional compared with semiconductors (for example, $K \approx 150$ W mK$^{-1}$ in bulk Si and $K \approx 10$ W mK$^{-1}$ in Si nanowires at room temperature[134]).

The explosive growth of the new field of thermal properties of graphene and low-dimensional carbons does not allow one to include all pertinent information in a single review. Unique characteristics, which were not discussed in detail, include graphene's negative thermal-expansion coefficient $\alpha = (-4.8\pm1.0) \times 10^{-6}$ K$^{-1}$ for $T < 300$ K, which switches sign at $T \approx 900$ K for single-layer graphene and $T \approx 400$ K for bilayer graphene[135]. These properties are rooted in the intricacies of the phonon dispersion in graphene and FLG[74,83,135–138]. One can expect that graphene's thermal properties can be strain-engineered in a similar way to its electronic properties[139]. Another important issue is the effect of the defects, grain size and orientation on $K(T)$ of graphene. Recently, two similar studies[140,141] suggested that $K(T)$ of $\sim T^{1.4}$ or $\sim T^{1.5}$ dependences prove that ZA modes are dominant in graphene heat transport. However, it is well known[29] that $K(T)$ dependence is strongly influenced by the material quality (Fig. 1b). The $K$ values below bulk graphite and $K(T)$ dependence in refs. 140,141 probably indicate polycrystalline graphene with small and misoriented grains or a high concentration of defects due to processing as suggested in ref. 142. Thermal contact resistance of graphene and CNTs, which can affect the accuracy of measurements and change $K$ values[142–144], also deserves more thorough consideration. It has been shown that $K$ of isotopically pure bulk diamond and Si can be substantially improved, compared with their natural abundance[145,146]. The isotope effects in graphene have been considered only computationally[83,147] and await experimental investigation. Theoretical approaches developed specifically for graphene thermal properties now appear on a regular basis. Recent calculations[148], which used density functional theory and the adaptive force matching method for graphene, found $K$ values in line with earlier reports[16,17,62,80,83,84]. Finally, the rise of graphene[13] has renewed interest in other carbon allotropes including their prospects for thermal management[55]. The use of complementary electronic and thermal properties of combinations of low-dimensional carbon materials makes the prospects of carbon or hybrid Si–C electronics much more feasible.

## References


1. Balandin, A. A. Better computing through CPU cooling. *IEEE Spectrum* 29–33 (October, 2009).
2. Ioffe, A. F. *Semiconductor Thermoelements and Thermal Cooling* (Nauka, 1956).
3. Borca-Tasciuc, T. *et al.* Thermal conductivity of InAs/AlSb superlattices. *Microscale Thermophys. Eng.* **5,** 225–231 (2001).
4. Balandin, A. & Wang, K. L. Significant decrease of the lattice thermal conductivity due to phonon confinement in a free-standing semiconductor quantum well. *Phys. Rev. B.* **58,** 1544–1549 (1998).
5. Lepri, S., Livi, R. & Politi, A. Thermal conduction in classical low-dimensional lattices. *Phys. Rep.* **377,** 1–80 (2003).
6. Basile, G., Bernardin, C. & Olla, S. Momentum conversion model with anomalous thermal conductivity in low dimensional system. *Phys. Rev. Lett.* **96,** 204303–204304 (2006).
7. Chang, C. W., Okawa, D., Garcia, H., Majumdar, A. & Zettl, A. Breakdown of Fourier's law in nanotube thermal conductors. *Phys. Rev. Lett.* **101,** 075903–075904 (2008).
8. Narayan, O. & Ramaswamy, S. Anomalous heat conduction in one dimensional momentum-conserving systems. *Phys. Rev. Lett.* **89,** 200601–200604 (2002).
9. Dresselhaus, M. S., Dresselhaus, G. & Eklund, P. C. *Science of Fullerenes and Carbon Nanotubes* (Academic Press, 1996).
10. Kim, P., Shi, L., Majumdar, A. & Mc Euen, P. L. Thermal transport measurement of individual multiwalled nanotubes. *Phys. Rev. Lett.* **87,** 215502 (2001).
11. Pop, E., Mann, D., Wang, Q., Goodson, K. & Dai, H. Thermal conductance of an individual single-wall carbon nanotube above room temperature. *Nano Lett.* **6,** 96–100 (2006).
12. Novoselov, K. S. *et al.* Electric field effect in atomically thin carbon films. *Science* **306,** 666–669 (2004).
13. Geim, A. K. & Novoselov, K. S. The rise of graphene. *Nature Mater.* **6,** 183–191 (2007).
14. Novoselov, K. S. *et al.* Two-dimensional gas of massless Dirac fermions in graphene. *Nature* **438,** 197–200 (2005).
15. Zhang, Y. B., Tan, Y. W., Stormer, H. L. & Kim, P. Experimental observation of the quantum Hall effect and Berry's phase in graphene. *Nature* **438,** 201–204 (2005).
16. Balandin, A. A. *et al.* Superior thermal conductivity of single layer graphene. *Nano Lett.* **8,** 902–907 (2008).
17. Ghosh, S. *et al.* Extremely high thermal conductivity in graphene: Prospects for thermal management application in nanoelectronic circuits. *Appl. Phys. Lett.* **92,** 151911 (2008).
18. Calizo, I., Balandin, A. A., Bao, W., Miao, F. & Lau, C. N. Temperature dependence of the Raman spectra of graphene and graphene multilayers. *Nano Lett.* **7,** 2645–2649 (2007).
19. Ghosh, S. *et al.* Thermal properties of polycrystalline graphene films and reduced graphene-oxide films. *MRS Proc.* **S6.2,** 198 (2010).
20. Bhandari, C. M. & Rowe, D. M. *Thermal Conduction in Semiconductors* (Wiley & Sons, 1988).
21. Cahill, D. G. Thermal conductivity measurement from 30 to 750 K: the 3ω method. *Rev. Sci. Instrum.* **61,** 802–808 (1990).

22. Klemens, P. G. *Solid State Physics* Vol. 7 (eds Seitz, F. & Turnbull, D.) 1–98 (Academic, 1958).
23. Klemens, P. G. Theory of the A-plane thermal conductivity of graphite. *J. Wide Bandgap Mater.* **7,** 332–339 (2000).
24. Pierson, H. O. *Handbook of Carbon, Graphite, Diamonds and Fullerenes: Processing, Properties and Applications* (Noyes Publications, 2010).
25. Callaway, J. Model for lattice thermal conductivity at low temperatures. *Phys. Rev.* **113,** 1046–1051 (1959).
26. Parrott, J. E. & Stuckes, A. D. *Thermal Conductivity of Solids* (Methuen, 1975).
27. Ziman, J. M. *Electrons and Phonons: The Theory of Transport Phenomena in Solids* (Oxford Univ. Press, 2001).
28. Balandin, A. & Wang, K. L. Effect of phonon confinement on the thermoelectric figure of merit of quantum wells. *J. Appl. Phys.* **84,** 6149–6153 (1998).
29. Ho, C. Y., Powell, R. W. & Liley, P. E. Thermal conductivity of the elements: a comprehensive review. *J. Phys. Chem. Ref. Data* **3** (suppl. 1), 1–30 (1974).
30. Woodcraft, A. L. *et al.* Thermal conductivity measurements of pitch-bonded at millikelvin temperatures: finding a replacement for AGOT graphite. *Cryogenics* **49,** 159–164 (2009).
31. Nelson, F. J. *et al.* Optical properties of large-area polycrystalline chemical vapour deposited graphene by spectroscopic ellipsometry. *Appl. Phys. Lett.* **97,** 253110 (2010).
32. Park, S. & Ruoff, R. S. Chemical methods for the production of graphenes. *Nature Nanotech.* **4,** 217–224 (2009).
33. Klemens, P. G. & Pedraza, D. F. Thermal conductivity of graphite in basal plane. *Carbon* **32,** 735–741 (1994).
34. Cahill, D. G. & Pohl, R. O. Heat flow and lattice vibrations in glasses. *Solid State Commun.* **70,** 927–930 (1989).
35. Robertson, J. Diamond like amorphous carbon. *Mater. Sci. Eng.* **R37,** 129–281 (2002).
36. Morath, C. J. *et al.* Picosecond optical studies of amorphous diamond and diamond-like carbon: Thermal conductivity and longitudinal sound velocity. *J. Appl. Phys.* **76,** 2636–2640 (1994).
37. Hurler, W., Pietralla, M. & Hammerschmidt, A. Determination of thermal properties of hydrogenated amorphous carbon thin films via mirage effect measurement. *Diam. Relat. Mater.* **4,** 954–957 (1995).
38. Zhang, Z. J., Fan, S., Huang, J. & Lieber, C. M. Diamond-like properties in single phase carbon nitride solid. *Appl. Phys. Lett.* **68,** 2639–2641 (1996).
39. Bullen, A. J., O'Hara, K. E., Cahill, D. G., Monteiro, O. & von Keudell, A. Thermal conductivity of amorphous carbon thin films. *J. Appl. Phys.* **88,** 6317–6320 (2000).
40. Chen, G., Hui, P. & Xu, S. Thermal conduction in metalized tetrahedral amorphous carbon (ta-C) films on silicon. *Thin Solid Films* **366,** 95–99 (2000).
41. Shamsa, M. *et al.* Thermal conductivity of diamond like carbon films. *Appl. Phys. Lett.* **89,** 161921 (2006).
42. Balandin, A. A., Shamsa, M., Liu, W. L., Casiraghi, C. & Ferrari, A. C. Thermal conductivity of ultrathin tetrahedral amorphous carbon. *Appl. Phys. Lett.* **93,** 043115 (2008).
43. Butler, J. E. & Sumant, A. V. The CVD of nanodiamond materials. *Chem. Vapor Depos.* **14,** 145–160 (2008).
44. Auciello, O. & Sumant, A. V. Status review of the science and technology of devices. *Diam. Relat. Mater.* **19,** 699–718 (2010).
45. Gruen, D. M., Liu, S., Krauss, A. R. & Pan, X. Buckyball microwave plasmas: Fragmentation and diamond-film growth. *J. Appl. Phys.* **75,** 1758–1763 (1994).
46. Hartmann, J., Voigt, P. & Reichling, M. Measuring local thermal conductivity in polycrystalline diamond with a high resolution photothermal microscope. *J. Appl. Phys.* **81,** 2966–2972 (1997).
47. Reichling, M., Klotzbucher, T. & Hartmann, J. Local variation of room-temperature thermal conductivity in high-quality polycrystalline diamond. *Appl. Phys. Lett.* **73,** 756–758 (1998).
48. Philip, J. *et al.* Elastic, mechanical and thermal properties of nanocrystalline diamond films. *J. Appl. Phys.* **93,** 2164–2171 (2003).
49. Angadi, M. A. *et al.* Thermal transport and grain boundary conductance in ultrananocrystalline diamond thin films. *J. Appl. Phys.* **99,** 114301 (2006).
50. Liu, W. L. *et al.* Thermal conduction in nanocrystalline diamond thin films: Effect of grain boundary scattering and nitrogen doping. *Appl. Phys. Lett.* **89,** 171915 (2006).
51. Shamsa, M. *et al.* Thermal conductivity of nitrogened ultrananocrystalline diamond films on silicon. *J. Appl. Phys.* **103,** 083538 (2008).
52. Khitun, A., Balandin, A., Liu, J. L. & Wang, K. L. In-plane lattice thermal conductivity of quantum-dot superlattice. *J. Appl. Phys.* **88,** 696–699 (2000).
53. Braginsky, L., Shklover, V., Hofmann, H. & Bowen, P. High-temperature thermal conductivity of porous $Al_2O_3$ nanostructures. *Phys. Rev. B* **70,** 134201 (2004).
54. Ferrari, A. C. & Robertson, J. Origin of the 1,150 $cm^{-1}$ Raman mode in nanocrystalline diamond. *Phys. Rev. B* **63,** 121405 (2001).
55. Goyal, V., Subrina, S., Nika, D. L. & Balandin, A. A. Reduced thermal resistance of the silicon-synthetic diamond composite substrate at elevated temperatures. *Appl. Phys. Lett.* **97,** 031904 (2010).
56. Saito, K. & Dhar, A. Heat conduction in a three dimensional anharmonic crystal. *Phys. Rev. Lett.* **104,** 040601 (2010).
57. Lippi, A. & Livi, R. Heat conduction in two-dimensional nonlinear lattices. *J. Stat. Phys.* **100,** 1147–1172 (2000).
58. Yang, L. Finite heat conduction in a 2D disorder lattice. *Phys. Rev. Lett.* **88,** 094301 (2002).
59. Dhar, A. Heat conduction in the disordered harmonic chain revisited. *Phys. Rev. Lett.* **86,** 5882–5885 (2001).
60. Casher, A. & Lebowitz, J. L. Heat flow in regular and disordered harmonic chains. *J. Math. Phys.* **12,** 1701–1711 (1971).
61. Klemens, P. G. Theory of thermal conduction in the ceramic films. *Int. J. Thermophys.* **22,** 265–275 (2001).
62. Nika, D. L., Ghosh, S., Pokatilov, E. P. & Balandin, A. A. Lattice thermal conductivity of graphene flakes: Comparison and bulk graphite. *Appl. Phys. Lett.* **94,** 203103 (2009).
63. Hone, J., Whitney, M., Piskoti, C. & Zettl, A. Thermal conductivity of single-walled carbon nanotubes. *Phys. Rev. B* **59,** R2514–R2516 (1999).
64. Yu, C. H., Shi, L., Yao, Z., Li, D. Y. & Majumdar, A. Thermal conductance and thermopower of an single-wall carbon nanotubes. *Nano Lett.* **5,** 1842–1846 (2005).
65. Fujii, M. *et al.* Measuring thermal conductivity of a single carbon nanotube. *Phys. Rev. Lett.* **95,** 065502 (2005).
66. Berber, S., Kwon, Y-K. & Tomanek, D. Unusually high thermal conductivity of carbon nanotubes. *Phys. Rev. Lett.* **84,** 4613–4616 (2000).
67. Che, J., Cagin, T. & Goddard, W. A. III Thermal conductivity of carbon nanotubes. *Nanotechnology* **11,** 65–69 (2000).
68. Osman, M. A. & Srivastava, D. Temperature dependence of thermal conductivity of single-wall carbon nanotubes. *Nanotechnology* **12,** 21–24 (2001).
69. Lindsay, L., Broido, D. A. & Mingo, N. Diameter dependence of carbon nanotube thermal conductivity and extension to the graphene limit. *Phys. Rev. B* **82,** 161402 (2010).
70. Donadio, D. & Galli, G. Thermal conductivity of isolated and interacting carbon nanotubes: Comparing results from molecular dynamics and the Boltzmann transport equation. *Phys. Rev. Lett.* **99,** 255502 (2007).
71. Chang, C. W. *et al.* Isotope effect on the thermal conductivity of boron nitride nanotubes. *Phys. Rev. Lett.* **97,** 085901 (2006).
72. Rego, L. C. G. & Kirczenow, G. Fractional exclusion statistics and the universal quantum of thermal conductance: A unifying approach. *Phys. Rev. B* **59,** 13080–13086 (1999).
73. Ghosh, S., Nika, D. L., Pokatilov, E. P. & Balandin, A. A. Heat conduction in graphene: Experimental study and theoretical interpretation. *New J. Phys.* **11,** 095012 (2009).
74. Ghosh, S. *et al.* Dimensional crossover of thermal transport in few-layer graphene. *Nature Mater.* **9,** 555–558 (2010).
75. Cai, W. *et al.* Thermal transport in suspended and supported monolayer graphene grown by chemical vapor deposition. *Nano Lett.* **10,** 1645–1651 (2010).
76. Faugeras, C. *et al.* Thermal conductivity of graphene in Corbino membrane geometry. *ACS Nano* **4,** 1889–1892 (2010).
77. Jauregui, L. A. *et al.* Thermal transport in graphene nanostructures: Experiments and simulations. *ECS Trans.* **28,** 73–83 (2010).
78. Seol, J. H. *et al.* Two-dimensional phonon transport in supported graphene. *Science* **328,** 213–216 (2010).
79. Murali, R., Yang, Y., Brenner, K., Beck, T. & Meindl, J. D. Breakdown current density of graphene nanoribbons. *Appl. Phys. Lett.* **94,** 243114 (2009).
80. Zhong, W. R., Zhang, M. P., Ai, B. Q. & Zheng, D. Q. Chirality and thickness-dependent thermal conductivity of few-layer graphene: A molecular dynamics study. *Appl. Phys. Lett.* **98,** 113107 (2011).
81. Singh, D., Murthy, J. Y. & Fisher, T. S. Mechanism of thermal conductivity reduction in few-layer graphene. Preprint at http://arxiv.org/abs/1104.4964 (2011).
82. Jang, W., Chen, Z., Bao, W., Lau, C. N. & Dames, C. Thickness-dependent thermal conductivity of encased graphene and ultrathin graphite. *Nano Lett.* **10,** 3909–3913 (2010).
83. Nika, D. L., Pokatilov, E. P., Askerov, A. S. & Balandin, A. A. Phonon thermal conduction in graphene: Role of Umklapp and edge roughness scattering. *Phys. Rev. B* **79,** 155413 (2009).
84. Evans, W. J., Hu, L. & Keblinsky, P. Thermal conductivity of graphene ribbons from equilibrium molecular dynamics: Effect of ribbon width, edge roughness, and hydrogen termination. *Appl. Phys. Lett.* **96,** 203112 (2010).
85. Lindsay, L., Broido, D. A. & Mingo, N. Flexural phonons and thermal transport in graphene. *Phys. Rev. B* **82,** 115427 (2010).
86. Munoz, E., Lu, J. & Yakobson, B. I. Ballistic thermal conductance of graphene ribbons. *Nano Lett.* **10,** 1652–1656 (2010).
87. Savin, A. V., Kivshar, Y. S. & Hu, B. Suppression of thermal conductivity in graphene nanoribbons with rough edges. *Phys. Rev. B* **82,** 195422 (2010).
88. Jiang, J-W., Wang, J-S. & Li, B. Thermal conductance of graphite and dimerite. *Phys. Rev. B* **79,** 205418 (2009).
89. Huang, Z., Fisher, T. S. & Murthy, J. Y. Simulation of phonon transmission through graphene and graphene nanoribbons with a green's function method. *J. Appl. Phys.* **108,** 094319 (2010).

90. Hu, J., Ruan, X. & Chen, Y. P. Thermal conductivity and thermal rectification in graphene nanoribbons: A molecular dynamic study. *Nano Lett.* **9,** 2730–2735 (2009).
91. Guo, Z., Zhang, D. & Gong, X-G. Thermal conductivity of graphene nanoribbons. *Appl. Phys. Lett.* **95,** 163103 (2009).
92. Chen, S. *et al.* Raman measurement of thermal transport in suspended monolayer graphene of variable sizes in vacuum and gaseous environments. *ACS Nano* **5,** 321–328 (2011).
93. Lee, J. U., Yoon, D., Kim, H., Lee, S. W. & Cheong, H. Thermal conductivity of suspended pristine graphene measured by Raman spectroscopy. *Phys. Rev. B* **83,** 081419 (2011).
94. Mak, K. F., Shan, J. & Heinz, T. F. Seeing many-body effects in single and few layer graphene: observation of two-dimensional saddle point excitons. *Phys. Rev. Lett.* **106,** 046401 (2011).
95. Huang, Y., Wu, J. & Hwang, K. C. Thickness of graphene and single-wall carbon nanotubes. *Phys. Rev. B* **74,** 245413 (2006).
96. Odegard, G. M., Gates, T. S., Nicholson, L. M. & Wise, K. E. Continuum model for the vibration of multilayered graphene sheets. *Compos. Sci. Technol.* **62,** 1869 (2002).
97. Kapitza, P. L. *Collected Papers of P. L. Kapitza* Vol. II (ed. ter Haar, D.) 581 (Pergamon Press, 1967).
98. Freitag, M. *et al.* Energy dissipation in graphene field effect transistors. *Nano Lett.* **9,** 1883–1888 (2009).
99. Chen, Z., Jang, W., Bao, W., Lau, C. N. & Dames, C. Thermal contact resistance between graphene and silicon dioxide. *Appl. Phys. Lett.* **95,** 161910 (2009).
100. Mak, K. F., Liu, C. H. & Heinz, T. F. Thermal conductance at the graphene-$SiO_2$ interface measured by optical pump-probe spectroscopy. Preprint at http://arxiv.org/abs/1009.0231 (2010).
101. Koh, Y. K., Bae, M-H., Cahill, D. G. & Pop, E. Heat conduction across monolayer and few-layer graphenes. *Nano Lett.* **10,** 4363–4368 (2010).
102. Schmidt, A. J., Collins, K. C., Minnich, A. J. & Chen, G. Thermal conductance and phonon transmissivity of metal-graphite interfaces. *J. Appl. Phys.* **107,** 104907 (2010).
103. Persson, B. N. J. & Ueba, H. Heat transfer between weakly coupled systems: Graphene on a-$SiO_2$. *Europhys. Lett.* **91,** 56001 (2010).
104. Konatham, D. & Striolo, A. Thermal boundary resistance at the graphene-oil interface. *Appl. Phys. Lett.* **95,** 163105 (2009).
105. Choi, S. U. S., Zhang, Z. G., Yu, W., Lockwood, F. E. & Grulke, E. A. Anomalous thermal conductivity enhancement in nanotube suspensions. *Appl. Phys. Lett.* **79,** 2252–2254 (2001).
106. Biercuk, M. J. *et al.* Carbon nanotube composite for thermal management. *Appl. Phys. Lett.* **80,** 2767–2769 (2002).
107. Konatham, D. & Striolo, A. Thermal boundary resistance at the graphene-oil interface. *Mol. Phys.* **109,** 97–111 (2011).
108. Yu, A., Itkis, M. E., Bekyarova, E & Haddon, R. C. Effect of single-walled carbon nanotube purity on the thermal conductivity of carbon nanotube-based composite. *Appl. Phys. Lett.* **89,** 133102 (2006).
109. Yu, A., Ramesh, P., Itkis, M. E., Bekyarova, E. & Haddon, R. C. Graphite nanoplatelet- epoxy composite thermal interface materials. *J. Phys. Chem. Lett.* **111,** 7565–7569 (2007).
110. Yu, W., Xie, H. & Chen, W. Experimental investigation on thermal conductivity of nanofluids containing graphene oxide nanosheets. *J. Appl. Phys.* **107,** 094317 (2010).
111. Wang, S., Tambraparni, M., Qiu, J., Tipton, J. & Dean, D. Thermal expansion of graphene composites. *Macromolecules* **42,** 5251–5255 (2009).
112. Shahil, K. M. F., Goyal, V. & Balandin, A. A. Thermal properties of graphene: Applications in thermal interface materials. *ECS Trans.* **35,** 193–195 (2011).
113. Zhang, K., Chai, Y., Yuen, M. M. F., Xiao, D. G. W. & Chan, P. C. H. Carbon nanotube thermal interface material for high-brightness light-emitting-diode cooling. *Nanotechnology* **19,** 215706 (2008).
114. Veca, L. M. *et al.* Carbon nanosheets for polymeric nanocomposites with high thermal conductivity. *Adv. Mater.* **21,** 2088–2092 (2009).
115. Kim, K. *et al.* High-temperature stability of suspended single-layer graphene. *Phys. Status Solidi* **11,** 302–304 (2010).
116. Lotya, M., King, P. J., Khan, U., De, S. & Coleman, J. N. Liquid phase production of graphene by exfoliation of graphite in surfactant/water solutions. *ACS Nano*. **4,** 3155–3162 (2010).
117. Segal, M. Selling graphene by the ton. *Nature Nanotech.* **4,** 612–614 (2009).
118. Zuev, Y. M., Chang, W. & Kim, P. Thermoelectric and magneto-thermoelectric transport measurements of graphene. *Phys. Rev. Lett.* **102,** 096807 (2009).
119. Wei, P., Bao, W., Pu, Y., Lau, C. N. & Shi, J. Anomalous thermoelectric transport of Dirac particles in graphene. *Phys. Rev. Lett.* **102,** 166808 (2009).
120. Checkelsky, J. G. & Ong, N. P. Thermopower and Nernst effect in graphene in a magnetic field. *Phys. Rev. B* **80,** 081413 (2009).
121. Hwang, E. H., Rossi, E. & Das Sarma, S. Theory of carrier transport in bilayer graphene. *Phys. Rev. B* **80,** 235415 (2009).
122. Bao, W. S., Liu, S. Y. & Lei, X. L. Nonlinear d.c. transport in graphene. *J. Phys. Condens. Mat.* **22,** 315502 (2010).
123. Kubakaddi, S. S. & Bhargavi, K. S. Enhancement of phonon-drag thermopower in bilayer graphene. *Phys. Rev. B* **82,** 155410 (2010).
124. Hu, J., Schiffli, S., Vallabhaneni, A., Ruan, X. & Chen, Y. P. Tuning the thermal conductivity of graphene nanoribbons by edge passivation and isotope engineering: A molecular dynamics study. *Appl. Phys. Lett.* **97,** 133107 (2010).
125. Makeev, M. A. & Srivastava, D. Silicon carbide nanowires under external loads: An atomistic simulation study. *Appl. Phys. Lett.* **95,** 181908 (2009).
126. Sevincli, H. & Cuniberti, G. Enhanced thermoelectric figure of merit in edge-disordered zigzag graphene nanoribbons. *Phys. Rev. B* **81,** 113401 (2010).
127. Teweldebrhan, D. & Balandin, A. A. Modification of graphene properties due to electron-beam irradiation. *Appl. Phys. Lett.* **94,** 013101 (2009).
128. Wang, D. & Shi, J. Effect of charged impurities on the thermoelectric power of graphene near the Dirac point. *Phys. Rev. B.* **83,** 113403 (2011).
129. Subrina, S., Kotchetkov, D. & Balandin, A. A. Heat removal in silicon-on-insulator integrated circuits with graphene lateral heat spreaders. *IEEE Electr. Device Lett.* **30,** 1281 (2009).
130. Kim, K. S. *et al.* Large-scale pattern growth of graphene films for stretchable transparent electrodes. *Nature* **457,** 706–710 (2009).
131. Reina, A. *et al.* Large area few-layer graphene films on arbitrary substrates by chemical vapor deposition. *Nano Lett.* **9,** 30–35 (2009).
132. Li, X. *et al.* Large-area synthesis of high-quality and uniform graphene films on copper foils. *Science* **324,** 1312–1313 (2009).
133. Yan, Z., Liu, G., Subrina, S. & Balandin, A. A. Experimental demonstration of efficient thermal management of high-power GaN/AlGaN transistors with graphene lateral heat spreaders. *MRS Proc.* Y3.5 (2011).
134. Zou J. & Balandin, A. A. Phonon heat conduction in a semiconductor nanowire, *J. Appl. Phys.* **89,** 2932–2938 (2001).
135. Zakharchenko, K. V., Los, J. H., Katsnelson, M. I. & Fasolino, A. Atomistic simulations of structural and thermodynamic properties of bilayer graphene. *Phys. Rev. B* **81,** 235439 (2010).
136. Mounet, N. & Marzari, N. First-principles determination of the structural, vibrational and thermodynamic properties of diamond, graphite, and derivatives. *Phys. Rev. B* **71,** 205214 (2005).
137. Michel, K. H. & Verberck, B. Theory of the evolution of phonon spectra and elastic constants from graphene to graphite. *Phys. Rev. B* **78,** 085424 (2008).
138. Shelling, P. K. & Keblinski, P. Thermal expansion of carbon structures. *Phys. Rev. B* **68,** 035425 (2003).
139. Pereira, V. M. & Castro-Neto, A. H. Strain engineering of graphene's electronic structure. *Phys. Rev. Lett.* **103,** 046801 (2009).
140. Xu, X. *et al.* Phonon transport in suspended single layer graphene. Preprint at http://arxiv.org/abs/1012.2937 (2010).
141. Wang, Z. *et al.* Thermal transport in suspended and supported few-layer graphene. *Nano Lett.* **11,** 113–118 (2011).
142. Pettes, M. T., Jo, I., Yao, Z. & Shi, L. Influence of polymeric residue on the thermal conductivity of suspended bilayer graphene. *Nano Lett.* **11,** 1195–1200 (2011).
143. Pettes, M. T. & Shi, L. Thermal and structural characterization of individual single-, double- and multi-walled carbon nanotubes. *Adv. Funct. Mater.* **19,** 3918–3925 (2009).
144. Hsu, I. K. *et al.* Optical measurement of thermal transport in suspended carbon nanotubes. *Appl. Phys. Lett.* **92,** 063119 (2008).
145. Capinski, W. S. *et al.* Thermal conductivity of isotopically enriched Si. *Appl. Phys. Lett.* **71,** 2109–2111 (1997).
146. Inyushkin, A. V., Taldenkov, A. N., Gibin, A. M., Gusev, A. V. & Pohl, H. J. *Ab initio* theory of the lattice thermal conductivity in diamond. *Phys. Status Solidi* **1,** 2995–2998 (2004).
147. Zhang, H. *et al.* Isotope effect on the thermal conductivity of graphene. *J. Nanomater.* **2010,** 537657 (2010).
148. Wei, D., Song, Y. & Wang, F. A. A simple molecular mechanics potential for mm scale graphene simulations from the adaptive force matching method. *J. Chem. Phys.* **134,** 184704 (2011).


## Acknowledgements

I am indebted to K. Saito, L. Lindsay, N. Mingo, C. Dames, R. S. Ruoff, L. Shi, N. Mounet, N. Marzari, B. Q. Ai and T. Heinz for providing figure files. I thank E. P. Pokatilov, D. Nika, C. Dames, L. Shi, D. Cahill, N. Mingo, R. S. Ruoff, P. Kim, J. Shi, M. Dresselhaus, A. Geim and K. Novoselov for useful discussions. This work was supported by the Office of Naval Research (ONR) through award N00014-10-1-0224, Semiconductor Research Corporation (SRC) and Defense Advanced Research Projects Agency (DARPA) through Focus Center Research Program (FCRP) Center on Functional Engineered Nano Architectonics (FENA), and DARPA Defense Microelectronics Activity (DMEA) under agreement H94003-10-2-1003. Past funding from US Air Force Office of Scientific Research (AFOSR) through contract A9550-08-1-0100 is also acknowledged.

## Author information

The author declares no competing financial interests.